Diagnosing and Remote Sealing of Leakage in Low-Pressure Sections of Natural Gas Distribution Networks

By

RANJITH NARASIMHAMURTHY
THESIS

Submitted in partial satisfaction of the requirements for the degree of

MASTER OF SCIENCE

in

Mechanical and Aerospace Engineering

in the

OFFICE OF GRADUATE STUDIES

of the

UNIVERSITY OF CALIFORNIA

DAVIS

Approved:

Mark Modera, Chair

Paul Erickson

Vinod Narayanan

Committee in Charge

2021

TABLE OF CONTENTS

LIST OF TABLES

LIST OF FIGURES

NOMENCLATURE

Conventional Symbols:

C_c	Cunningham correction factor	$-$
d_p	Diameter of the particle	m
d_t	Diameter of the duct (pipe)	m
f	Friction Factor	$-$
g	Acceleration due to gravity	m/s^2
L	Length of the duct (pipe)	m
m	Mass of gas	kg
$m_{internal}$	Mass of air in the system	kg
$\dot{m}_{standard}$	Mass Flow at standard conditions	kg/s
$\dot{m}_{actual}$	Mass Flow at actual conditions	kg/s
$\dot{m}_{internal}$	Rate of change of mass of air inside the system	kg/s
$\dot{m}_{in}$	Mass flow rate of air entering the system	kg/s
$\dot{m}_{out}$	Mass flow rate of air escaping from the leaks in the system	kg/s
$P_{barometric}$	Barometric (Atmospheric) Pressure of air	Pa
$P_{standard}$	Standard Absolute Pressure of 101325 Pa	Pa
P_{actual}	Actual Absolute Pressure of air in the system	Pa
$\dot{Q}_{standard_{air}}$	Volume flow rate of air at standard conditions of temperature and pressure	m^3/s
$T_{standard}$	Standard Temperature of 298 K	K
T_{actual}	Temperature at actual conditions	K

$P_{penetration}$	Penetration efficiency in a straight section	$-$
R_{air}	Ideal Gas Constant of air	$J/mol/K$
Re	Reynolds Number	$-$
T	Temperature of air in the system	K
U	Leak Rate of air in the system	$m^3/s/Pa$
$U_{velocity}$	Average Velocity of air in the duct (pipe)	m/s
V	Volume of air in the system	m^3
V_e	Average deposition velocity	m/s
V_d	Particle Velocity due to turbulent diffusivity	m/s
V_g	Limiting particle velocity due to gravity	m/s
$\dot{v}_{standard}$	Volume Flow at standard conditions of temperature and pressure (Mass flow rate)	m^3
$\dot{v}_{actual}$	Volume Flow at actual conditions of temperature and pressure (Volumetric flow rate)	m^3

Greek Symbols:

$\rho_{standard_{air}}$	Density of air at standard conditions of 298 K and 101325 Pa	kg/m^3
$\rho_{standard}$	Density at standard conditions of temperature and pressure	kg/m^3
ρ_{actual}	Density at actual conditions of temperature and pressure	kg/m^3
ρ_p	Density of the particle	kg/m^3
μ_a	Absolute viscosity of air	$kg/m/s$
τ	Particle Relaxation Time	s

ACKNOWLEDGEMENTS

My thesis would be incomplete if I did not thank all the people who have been a vital part of my master's journey and helped me see light at the end of the tunnel.

I would like to extend my deepest gratitude to Prof. Mark Modera for giving me this opportunity to work under his wonderful mentorship and guidance. I have learnt so much from you in the past two years and would definitely carry these lessons with me throughout my career and life. I thank you for being patient with me and guiding me with insightful comments and advice in every step of this journey.

I would like to thank Theresa Pistochini for allowing me to work on multiple projects at the WCEC; the time I spent at WCEC have been an important learning experience for me. I would also like to thank all the staff at WCEC for always being ready to extend a helping hand whenever I had a question.

I would like to thank Prof. Paul Erickson and Prof. Vinod Narayanan for agreeing to be on my master's thesis committee and providing me with extremely valuable feedback.

I owe everything I am today to my family. I would like to thank Amma, Nana and Viswa for being my constant source of love, happiness and motivation. Thank you for always having my back and supporting me selflessly.

I would like to thank my friends Adithan, Akshay, Apoorva, Premikaa, Shreya, Sravani and Trivikram for making my life in grad school a little more joyous and significant, in spite of being time zones apart. I would also like to thank my friends in Davis for encouraging and supporting me whenever I needed it.

ABSTRACT

Residential natural gas is estimated as responsible for almost 15% of California's total methane (CH_4) emissions from natural gas. It is not known what fraction of these emissions is due to fugitive leaks in the low-pressure portions of the natural gas distribution network. This research aimed to diagnose and potentially seal leakage in the low-pressure portions of natural gas distribution networks by using aerosols. This included developing and testing protocols for measuring leakage downstream of the meter in houses and commercial buildings, applying those protocols in 10 different locations, designing a system to seal leaks in those systems remotely, and applying the sealing process in a make-shift pipe network. Only 2 out of the 10 locations tested were above the leakage detection limit in unsealed networks; the variation in gas temperature posed a challenge to diagnosing the leakage rates. The aerosol process employed for remote sealing appeared to be capable of sealing leaks in natural gas distribution pipes but will require more refinement to address the extremely low leakage levels observed in this study.

1. INTRODUCTION

Natural gas has wide residential usage for cooking, water heating and space heating, and is constituted mainly of methane (CH_4) (90%). CH_4 is a potent greenhouse gas (GHG) which has a global warming potential (GWP) of approximately 25 times that of Carbon-Dioxide (CO_2). With approximately 15% of California's natural gas CH_4 emissions being contributed by the residential sector, mitigation of methane emissions from residential natural gas distribution systems is an important step towards achieving California's ambitious climate change goals of reducing the GHG emissions by 40% below the 1990 levels by 2030 (Fischer et al., 2018). While emissions from the production and distribution of natural gas are well studied (Allen et al., 2013; Hendrick et al., 2016; Lamb et al., 2016), there have been a relatively few studies that address post-meter CH_4 emissions. One study that addressed post-meter CH_4 emissions suggested leak repair as a potential solution to mitigate the emissions (Fischer et al., 2018).

(Modera & Carrie, 1999) developed a method to remotely and non-invasively seal leaks in ducts using an aerosol. The aerosol sealing technology is based upon injecting a fog of aerosolized sealant particles in a pressurized enclosure (e.g., CH_4 distribution piping) where the pressure is within a target range. Particle size, drying characteristics, air velocity, and pressure determine the efficacy of the sealing process. Apart from being able to seal leaks remotely, this technology allows for automatic tracking of the sealing process, providing real-time feedback to the applicator, and documentation of the sealing performed. (Carrié & Modera, 2002) experimentally investigated the deposition of aerosol on slot- and joint-type leaks, both of which are commonly observed in HVAC air distribution systems. While this technology has been commercialized for

duct sealing and building envelope sealing (Harrington & Modera, 2013, 2014; Modera et al., 1996), it has only seen limited testing for natural gas distribution sealing.

An unpublished research previously conducted[1] showed that it was possible to seal 3 mm (1/8 $inches$) diameter leaks more than 38 m (125 ft) away from the aerosol injection point using a mock-up nominal 40 mm (1.6 $inch$es) diameter pipe. Building up on these results, the focus of the current study is to understand the leakage in the distribution networks downstream of the residential natural gas meters. This included developing a protocol to test leakage downstream of the meter in natural gas networks in residential and commercial facilities, measuring and quantifying the leakage in 10 residential natural gas systems, designing an aerosol sealing apparatus to remotely seal leaks in a natural gas piping network and sealing an example network to demonstrate the efficacy of the process.

[1] Work was compiled in a final report submitted to the California Energy Commission Energy Innovations Small Grant Program. Please refer to Appendix A. For further inquiries, contact Jean-Pierre Delplanque: (530) 754-6950 – delplanque@ucdavis.edu or Mark Modera: (530) 754-7671 – mpmodera@ucdavis.edu

2. METHODOLOGY

2.1 LEAKAGE DIAGNOSIS

2.1.1 Mass Flow and Volumetric Flow

In the industry, mass flow is commonly specified in terms of the volumetric flow at standard temperature and pressure conditions (a temperature of 298 K (25 $°C$) and an absolute pressure of 101325 Pa (14.696 PSI)). The volumetric flow at actual temperature and pressure can be normalized using the measured temperature and pressure data to calculate volumetric flow at standard conditions. This study would refer to the volumetric flow at standard conditions as 'mass flow rate' and the volumetric flow at actual conditions as 'volumetric flow rate'. Equation 2.1 describes the relation between the mass flow rate and the volumetric flow rate.

$$\dot{v}_{standard} = \dot{v}_{actual} * \frac{T_{standard}}{P_{standard}} * \frac{P_{actual}}{T_{actual}} \quad (2.1)$$

2.1.2 Lab testing

The goal of testing the leakage of unsealed joints in the laboratory was to identify the relationship between pressure and flow and identify an appropriate way to quantify the leakage of natural-gas networks. The experiments were conducted at both high and low pressures and the apparatus used for each of those were slightly different (Figure 2.1)

The equipment common to both the tests at high and low pressures were:

- Compressor: to supply compressed air required for steady state flow testing
- Compressed Air Tubing: to transport the compressed air
- Filter Drier: to filter out any dirt in the compressed air line and to dry out any condensation

- Pipe fittings to build a sample network for testing the leaks

Specific equipment used for testing at High Pressure Ranges were :

- Alicat Mass Flow Meter: to measure the amount of compressed air supplied and the pressure in the network
- Needle Valve: to control the amount of compressed air supplied

Specific equipment used for testing at Low Pressure Ranges were:

- Alicat Mass Flow Controller: to control the amount of compressed air injected (measured pressure differentials are outside the measurable range)
- Energy Conservatory DG-500 Digital Pressure Gauge: to measure the pressure in the network

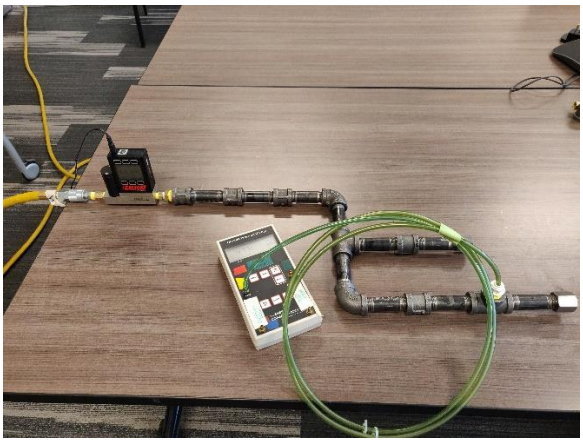

a.

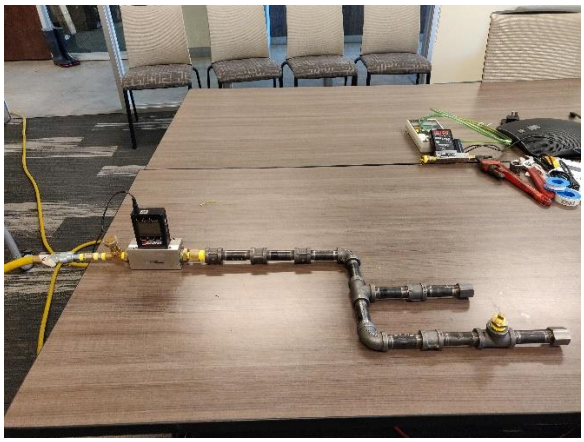

b.

Figure 2.1 a. Leak Testing apparatus for low pressure ranges b. Leak Testing apparatus for high pressure ranges

Steady-state leak testing was conducted on different systems to analyze the relationship between flow and pressure at high- and low-pressure ranges. In each trial of the experiment, a particular flow was supplied, and the system was allowed to stabilize to a particular pressure value, both of which were recorded. The process was then repeated for multiple flow values until the dataset was sufficiently populated.

Prior to performing the steady-state leak tests, a repeatability test was conducted to confirm that there were no other external factors like dirt, or water that would be affecting the experiment as time progressed. Although a filter drier was used for eliminating any dirt or water, it seemed best to confirm the repeatability of the pressure and flow values before proceeding to take the actual readings for multiple scenarios. For the repeatability test, the steady state leak tests were repeated multiple times on the same system with 1 ft of piping and 10 unsealed joints; the flow versus pressure observations were plotted to check for repeatability of the values. Refer to section 3.1.1 for results of the repeatability test.

Figure 2.2 System used for repeatability tests- 1 ft of pipe with 10 unsealed joints

2.1.3 Estimation of network volume from pressure decay data and measured leakage

A mass balance on the natural gas network pressurized with air and observed for a pressure decay would yield:

$$Rate\ of\ change\ of\ mass\ inside\ the\ system = Sum\ of\ mass\ flows\ entering\ and\ leaving\ the\ system \tag{2.2}$$

$$\dot{m}_{internal} = \dot{m}_{in} - \dot{m}_{out} \tag{2.3}$$

When the system is only decaying, there is no mass entering the system. Thus,

$$\dot{m}_{in} = 0 \tag{2.4}$$

$$\dot{m}_{internal} = -\dot{m}_{out} \tag{2.5}$$

The mass flow rate of air escaping from the system can be further simplified as:

$$\dot{m}_{out} = \dot{Q}_{standard_{air}} . \rho_{standard_{air}} \tag{2.6}$$

The ideal gas equation is expressed as follows:

$$m_{internal} = \frac{P_{actual} . V}{R_{air} . T} \tag{2.7}$$

Substituting equation 2.6 and 2.7 in 2.5,

$$\frac{d\left[\frac{P_{actual} . V}{R_{air} . T}\right]}{dt} = -\dot{Q}_{standard_{air}} . \rho_{standard_{air}} \tag{2.8}$$

From lab test results (Section 3.1.1), we found that the flow rate can be expressed as:

$$\dot{Q}_{standard_{air}} = U . (P_{actual} - P_{barometric}) \tag{2.9}$$

Where U is the slope of the flow rate versus pressure curve.

Equation 2.9 can be expressed as:

$$\frac{d\left[\frac{P_{actual} . V}{R_{air} . T}\right]}{dt} = -U . (P_{absolute} - P_{barometric}) . \rho_{standard_{air}} \tag{2.10}$$

$$\frac{d\left[\frac{(P_{actual}-P_{barometric}).V}{R_{air}.T}\right]}{dt}+\frac{d\left[\frac{P_{barometric}.V}{R_{air}.T}\right]}{dt} \tag{2.11}$$

$$=-U.(P_{actual}-P_{barometric}).\rho_{standard_{air}}$$

Let us assume that $P_{barometric}$ is a constant throughout (We will investigate the validity of this assumption in section 4.1.1). This would result in its derivative with respect to time be equal to 0. Thus,

$$\frac{d\left[\frac{(P_{actual}-P_{barometric}).V}{R_{air}.T}\right]}{dt}=-U.(P_{actual}-P_{barometric}).\rho_{standard_{air}} \tag{2.12}$$

$$\frac{d[(P_{actual}-P_{barometric})]}{P_{gauge}}=-\frac{U.\rho_{standard_{air}}.R_{air}.T}{V}dt \tag{2.13}$$

Temperature assumption: The temperature of the gas in the natural gas network can greatly vary based on the location of the network, i.e., the temperature of piping in the attic would be higher than the temperature of piping in the walls of the hallway. Although these temperature variations would affect the pressure of the gas in the network, it is generally impractical to measure the temperature at each individual location and account for the variation in pressure with temperature. Thus, for the sake of simplifying the analysis, the gas in the network is assumed to be a constant at 298 K. Equation 2.15 assumes that the temperature inside the network does not change with time.

Integrating on both sides,

$$\int\frac{d[(P_{actual}-P_{barometric})]}{P_{gauge}}=\int-\frac{U.\rho_{standard_{air}}.R_{air}.T}{V}dt \tag{2.14}$$

$$\int\frac{d[(P_{actual}-P_{barometric})]}{P_{gauge}}=-\frac{U.\rho_{standard_{air}}.R_{air}.T}{V}\int dt \tag{2.15}$$

$$\log((P_{actual} - P_{barometric})) + \log(c1) = -\frac{U.\rho_{standard_{air}}.R_{air}.T}{V}.t + \log(c2) \quad (2.16)$$

Where c1 and c2 are constants of integration.

$$\log((P_{actual} - P_{barometric})) + \log(c1) - \log(c2) = -\frac{U.\rho_{standard_{air}}.R_{air}.T}{V}.t \quad (2.17)$$

$$\log((P_{actual} - P_{barometric})) + \log(c1/c2) = -\frac{U.\rho_{standard_{air}}.R_{air}.T}{V}.t \quad (2.18)$$

$$\log\left((P_{actual} - P_{barometric}).\left(\frac{c1}{c2}\right)\right) = -\frac{U.\rho_{standard_{air}}.R_{air}.T}{V}.t \quad (2.19)$$

$$(P_{actual} - P_{barometric}).\left(\frac{c1}{c2}\right) = e^{-\frac{U.\rho_{standard_{air}}.R_{air}.T}{V}.t} \quad (2.20)$$

$$(P_{actual} - P_{barometric}) = \left(\frac{c2}{c1}\right).e^{-\frac{U.\rho_{standard_{air}}.R_{air}.T}{V}.t} \quad (2.21)$$

The above equation can be simplified and expressed as

$$(P_{actual} - P_{barometric}) = ce^{-A.t} \quad (2.22)$$

Where,

$$c = \frac{c2}{c1} \quad (2.23)$$

$$A = \frac{U.\rho_{standard_{air}}.R_{air}.T}{V} \quad (2.24)$$

Equation 2.22 is the general form of a pressure decay.

To estimate the volume of the gas network from the pressure decay, the following procedure is carried out:

1. An exponential trendline equation is obtained from the pressure decay curve of the system being tested
2. Constants c and A are calculated from the trendline equation
3. The leak rate U, measured from the mass flow leak test, is substituted along with the other constants in Equation 2.24, to calculate the volume V

2.1.4 Field Testing

Field testing was conducted to measure and quantify leakage in natural gas networks downstream of the meter, using and improvising on the techniques developed in the lab testing phase.

The apparatus for measuring the leakage (Figure 2.2) consists of the following:

- Mass Flow Controller: To control the mass flow rate of the compressed air injected into the network
- Differential Pressure Gauge: To measure the gauge pressure of the gas/compressed air in the network
- Temperature Sensor: To measure the temperature of the gas/compressed air in the network, just downstream of the flow meter
- Barometric Pressure Sensor: To measure the absolute pressure of the atmosphere surrounding the network
- Compressor: To supply compressed air to pressurize the network

Both pressure decay tests and steady state leak tests were carried out to comprehensively quantify the leakage of the system.

In a pressure decay test, the system is pressurized to a target pressure value and the pressure profile is observed; a decay is an indication of a leak. A Pressure Decay profile is recorded for three reasons:

- To confirm the presence of a measurable leak in the system
- To calculate a leak rate based on the geometrically estimated system volume
- To calculate a system volume based on the leak rate measured from the steady-state mass flow testing

a. b.

Figure 2.2 Field Experimental Apparatus for Leak Testing

In steady state leak testing, the natural gas network is supplied with a steady flow of compressed air and the pressure is allowed to stabilize to a steady-state value. Two sets of experiments are conducted: one including the flexible piping that goes to the appliances in the natural gas systems and another excluding the flexible lines by closing the supply valves upstream of the flexible lines and appliances. The leak rate is expressed as a ratio of the mass flow rate in standard milliliters per day to the gauge pressure in Pascals, i.e., $\frac{standard\ mL/day}{Pa}$.

NOTE: Flexible piping used in natural gas systems had a pressure limit of roughly 3500 Pa (0.50 PSI). Thus, the pressure in the network while injecting air should always be maintained below 3500 Pa.

A step-by-step protocol that was used for testing the networks has been outlined below:

1. Identify appliances connected to the gas line
2. Close burner valves, if any

3. Turn off pilot lights, if any
4. Locate a suitable place for connecting the leak testing apparatus (referred to as test location)
5. Turn off the main gas supply valve
6. Close the gas supply valve at test location
7. Disconnect appliance from test location
8. Connect the leak testing apparatus to the test location
9. Turn on the gas supply valve at the test location
10. Observe and record pressure and temperature profile for 30-90 minutes (until there is adequate decay time to calculate a time constant)
11. If there is **NO discernible decay**, (e.g. pressure increases or oscillates) ⇨
    a. Try cooling down the piping
    b. Record pressure and temperature profile again
12. If there is **a discernible decay**, then perform a mass flow leak test: ⇨
    a. Close all the shut-off valves to flexible lines and gas appliances
    b. Connect the compressor
    c. Inject compressed air at a steady mass flow rate (e.g. using mass flow controller) until pressure stabilizes
    d. Record the mass flow and pipe network pressure
    e. If we cannot get a stable reading after 30 minutes of trying, proceed to 13
    f. Repeat c and d at another flow and pressure **(Target pressure < 3500 Pa [0.5 PSI])**
13. If there is **a discernible decay**, then perform a mass flow leak test AGAIN: ⇨

a. Open the shut-off valves to flexible lines to all appliances connected to the natural gas network (other than at the test location)
b. Repeat 12 c to f **(Target pressure < 3500 Pa [0.5 PSI])**
c. Set the mass flow controller to zero
d. Disconnect the compressed air line
e. Close all the shut-off valves to flexible lines and gas appliances
f. Repeat Step 10

14. Close gas supply valve at the test location
15. Remove the leak testing apparatus and depressurize the compressor
16. Reconnect the appliance to the test location
17. Turn on the main gas supply valve
18. Relight pilot lights as needed (NOTE: it could take a while for the compressed air to be purged from the network)
19. Turn on burner valves as needed
20. Test that all appliances are working properly before leaving

2.2 LEAKAGE SEALING

2.2.1 Penetration model

(Anand & Mcfarland, 1989) developed a model to calculate the particle deposition in aerosol sampling lines because of turbulent diffusion and gravitational settling. The model makes three assumptions – particle concentration is uniform across the cross section of the tube section at any downstream location, flow is fully developed (either laminar or turbulent), thermo-physical properties of air and the aerosol particles are assumed to remain constant. Based on these assumptions, the reported value of penetration of aerosol through the tube is calculated as:

$$P_{penetration} = \mathrm{e}^{\frac{-4*V_e*L}{U_{velocity}*d_t}} \tag{2.25}$$

(Anand et al., 1992) provides a closed form solution of V_e:

$$V_e = \begin{cases} \frac{1}{2*\pi}\left[(\pi + 2*\gamma)*V_d + 2*V_g*\cos(\gamma)\right], & if\ |V_d| < |V_g|, \gamma = \operatorname{asin}\left(\frac{V_d}{V_g}\right) \\ V_d & if\ |V_d| \geq |V_g| \end{cases} \tag{2.26}$$

V_e is the vector sum of V_d and V_g.

The velocity caused by turbulent diffusion, V_d, was calculated based upon the models of (Agarwal, 1975) as follows:

$$V_d = V_* * U_{velocity} * \sqrt{\frac{f}{2}} \tag{2.27}$$

$$V_* = \begin{cases} 6.9 * 10^{-4}\tau_*^2, & if\ \tau_* \leq 15 \\ \frac{0.16}{\tau_*^{0.086}}, & if\ \tau_* > 15 \end{cases} \quad (2.28)$$

$$\tau_* = \frac{\tau U_{velocity}}{d_t} * f * Re \quad (2.29)$$

$$f = \frac{0.316}{4 * Re^{0.25}} \quad (2.30)$$

$$\tau = \frac{C_c \rho_p d_p^2}{18 * \mu_a} \quad (2.31)$$

A Cunningham's slip correction factor (C_c) of unity was used (i.e., the correction was neglected), since there would not be significant improvement of the model when the correction is applied (Anand & Mcfarland, 1989).

The terminal particle velocity due to gravitational settling, V_g, is based upon Stokes' Law and is given by:

$$V_g = g\tau \quad (2.32)$$

Now consider the case of laminar flow in a circular tube. Particles would deposit on the walls of the tube only due to gravitational settling. Therefore, substituting $V_d = 0$ in the equation 2.32 is equivalent to saying that the deposition is solely due to the contribution of gravitational settling. Doing so returns the following expression for V_e for laminar flow:

$$V_e = \frac{V_g}{\pi} \quad (2.33)$$

2.2.2 Lab Testing

A sample gas network as shown in Figure 2.3 was constructed to measure the extent to which the leakage of the network could be reduced using an aerosol sealing process. The leakage was measured before and after the sealing process by connecting the leak testing apparatus as shown in Figure 2.4. The network was set up to represent the components generally found in a residential natural gas network: 12.7 mm (½ $inches$) and 19.1 mm (¾ $inches$) metal piping, flexible piping, and valves.

The sealing equipment (see Figure 2.5) consisted of a wand, lay-flat plastic tubing and a wooden box. The lay-flat tubing creates a temporary disposable plastic tube that is used for capturing the spray of sealant and compressed air used for atomization. The wand is responsible for aerosolizing and spraying the sealant into the lay flat section; it consists of a liquid sealant line, a compressed air line, an in-line heater for the compressed air, and a temperature sensor to assure that the compressed-air line does not overheat. The sealant is sprayed into a 3 m (10 ft) long section of lay flat tubing that facilitates the process of evaporating the water from the water-based sealant, so as to produce dry sticky sealant particles. The sealant utilized was the same sealant that is currently used commercially to leaks in HVAC duct systems. It is a vinyl acetate polymer suspended in water, at a solids content of 35%. The wooden box was used to split the airflow into 3 different streams to connect to the 3 different entries into the pipe network. This is the manner by which one might seal a residential network in the field, entering at each appliance, and exiting at the point where the natural gas would normally enter the network (i.e., just downstream of the meter in normal operation). Section 4.2.3 proposes a methodology to seal a residential natural gas network.

Conventionally, sealing processes have used a fan to provide the required flow rates; this is because the flow rates required in duct systems were higher than the flow rate limit of compressors. But since our application required a lower flow rate and the compressor was anyway being used to aerosolize the sealant, it made sense to conduct the experiment with the compressor. Section 3.2.3 (Designing the Sealing Process) describes the flows observed in gas pipelines, in more detail.

Since only the compressed air line was used to provide air flow, it was imperative to run the sealant pump at a low enough flow rate so as to not saturate the air entering the network, and to produce smaller particles, so as to maximize the penetration efficiency of the particles in the network. The penetration efficiency of sealant particles over a given length of piping is defined as the ratio of concentration of sealant particles that reach the given length compared to the concentration of particles injected at the inlet of the pipe. The pump was operated at 20 $revolutions\ per\ minute$ (RPM), which translates to a flowrate of 4 CCM, or 0.24 kg/h. At the compressed-air pressure provided to the nozzle it moves roughly 170 $SLPM$ (6 $SCFM$), or 12 kg/h, resulting in an air to liquid sealant mass flow ratio of ~50. The mean particle size produced by this apparatus was estimated based upon testing results for the droplet sizes provided by the company that manufactures the duct-sealing nozzles employed for this experiment. These results were extrapolated using the trendline equation in Figure 2.6 for the operating conditions of the experiment. It is also to be noted that for a vinyl acetate polymer suspended in water, at a solids content of 35%, the particle sizes are 70% of the droplet sizes. The mean particle size thus estimated was about 6 μm for the operating conditions used in this study. The manufacturer also directly measured the particle size - simulating a pump speed of 20

RPM and a compressed-air pressure of 170 $SLPM$ - and estimated the particle size to be around 6.3 μm, which is in close agreement to the extrapolated value.

During the sealing process, the end of the network was capped until the pressure in the network reached the 3500 Pa (0.5 PSI) gauge pressure limit for flexible lines. Once this limit was reached, the cap was removed to provide pressure relief (Figure 2.3 a).

a. b.

Figure 2.3 Example natural gas network used for testing aerosol sealing process

Figure 2.4 Leak testing apparatus connected to example pipe network used for testing aerosol sealing process

a.

b.

Figure 2.5 Sealing Test Apparatus used to test aerosol sealing process

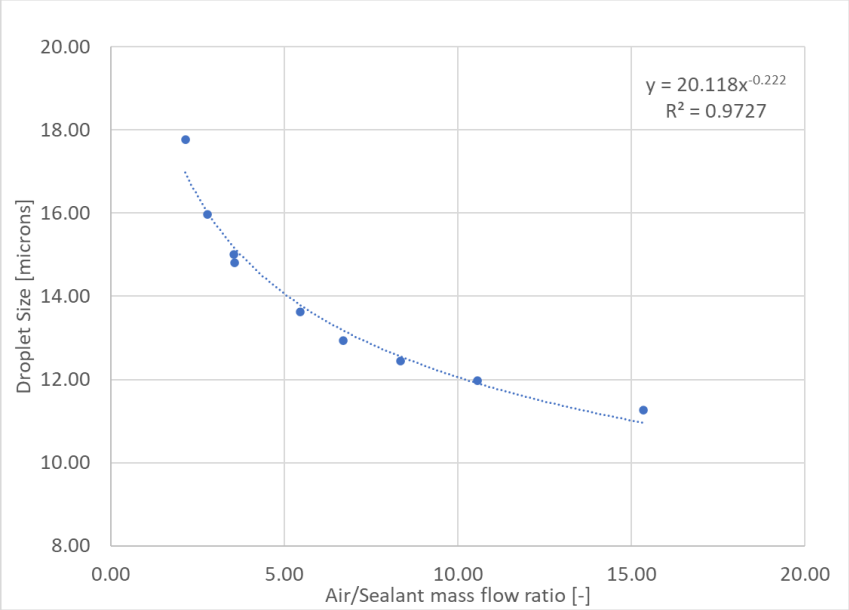

Figure 2.6 Droplet size versus mass flow ratio graph for the duct sealing nozzles employed in this experiment

3. RESULTS

3.1 LEAKAGE DIAGNOSIS

3.1.1 Lab Testing

Figure 3.1 compares the pressure-flow values for the same system repeated 5 times one after the other; the values show a high degree of overlap and repeatability. The results of the repeatability test provided the author with confidence that our apparatus would not be affected by any external factors which would distort the readings after every trial and was good to conduct further experiments.

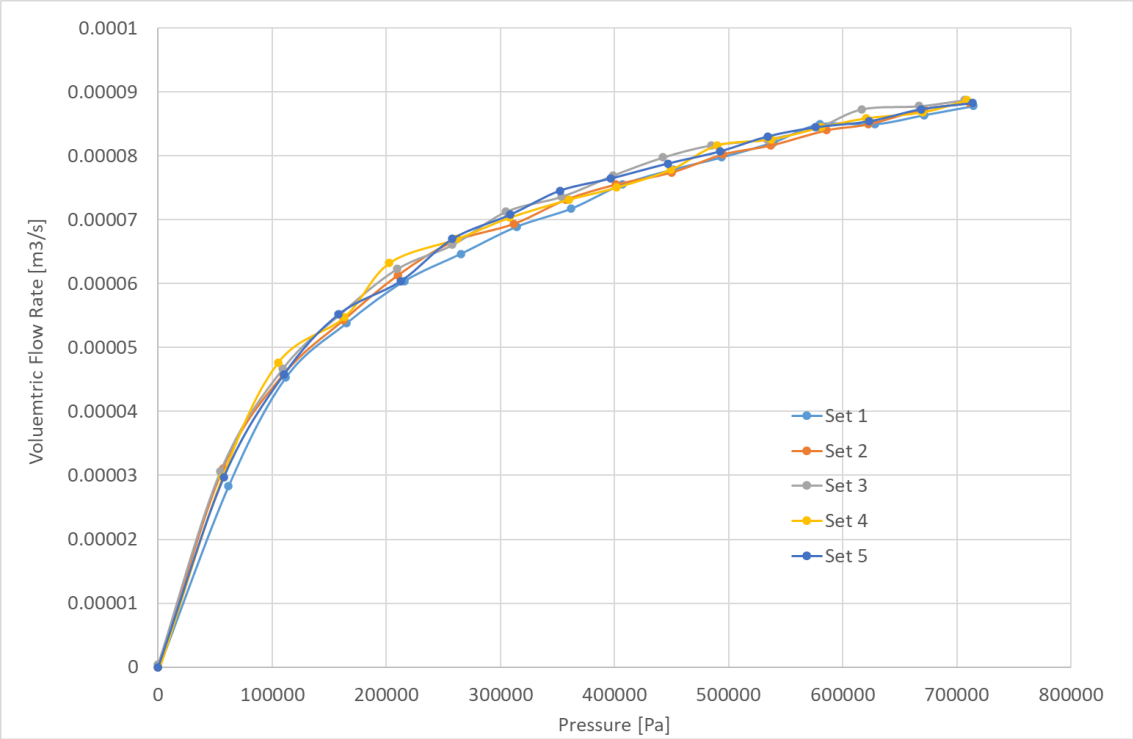

Figure 3.1 Repeatability tests for laboratory leak testing – 1 ft of pipe with 10 unsealed joints

For different system configurations, the variation of pressure with flow was recorded and plotted. For the sake of this analysis, the threads in a joint were covered with Teflon tape to simulate a sealed joint. Any reference to 'sealed' in this section refers to sealing with a Teflon tape.

Figure 3.3 compares the mass flow rates and volumetric flow rates of the two networks depicted in Figure 3.2 at low pressure of 0-1500 Pa. It can be observed that the mass flow rate and volumetric flow rate overlap for each individual network. The trend for both the mass flow rate and volumetric flow rate is linear. As expected, network 2, which has 20 unsealed joints and 0 sealed joints is leakier than network 1, which has 17 unsealed joints and 3 sealed joints. This can be seen in Figure 3.3 where at any given pressure, the flow rate of network 2 is higher than the flow rate of network 1.

When considering higher pressures, there is a stark difference between mass flow rates and volumetric flow rates. Figure 3.4 shows the 3 networks tested at high pressures. The mass flow rates, shown in Figure 3.5 depict a linear trend even at higher pressures. On the other hand, the volumetric flow rates significantly deviate from linearity (Figure 3.6) at higher pressures.

At low pressures and temperatures, the volumetric flow and mass flow rates are nearly identical. Since air is compressible, a drastic increase in the pressure and temperature affects the volume directly. As a result, the volumetric flow starts to deviate from the linear trend as the effect of temperature and pressure increase. On the other hand, the mass flow has already been normalized to a standard temperature and pressure and thus, keeps the linear trend.

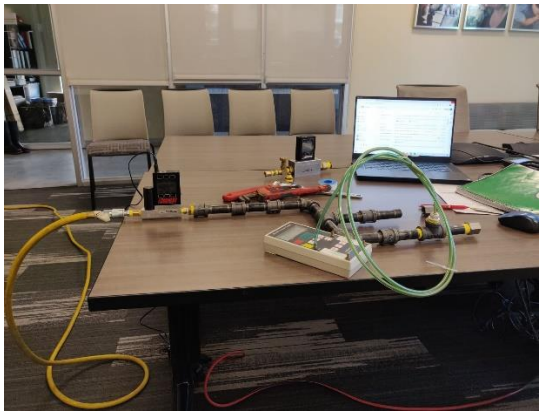

a.

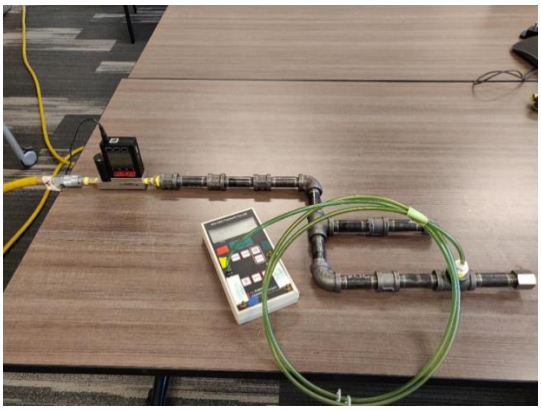

b.

Figure 3.2 a. Network 1 with 17 unsealed joint and 3 sealed joints b. Network 2 with 20 unsealed joints and 0 sealed joints

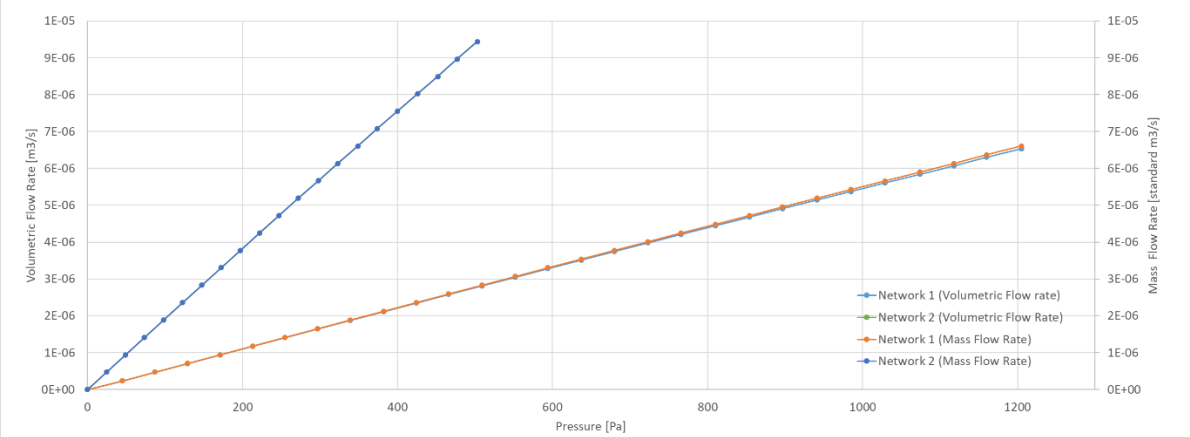

Figure 3.3 Comparison of Volumetric Flow Rate with Mass Flow Rate in the two networks shown in Figure 3.2 at low pressures of 0-1500 Pa

a. b. c.

Figure 3.4 a. Network 3 with 8 unsealed joints and 2 sealed joints b. Network 4 with 7 unsealed joints and 3 sealed joints c. Network 5 with 6 unsealed joints and 4 sealed joints

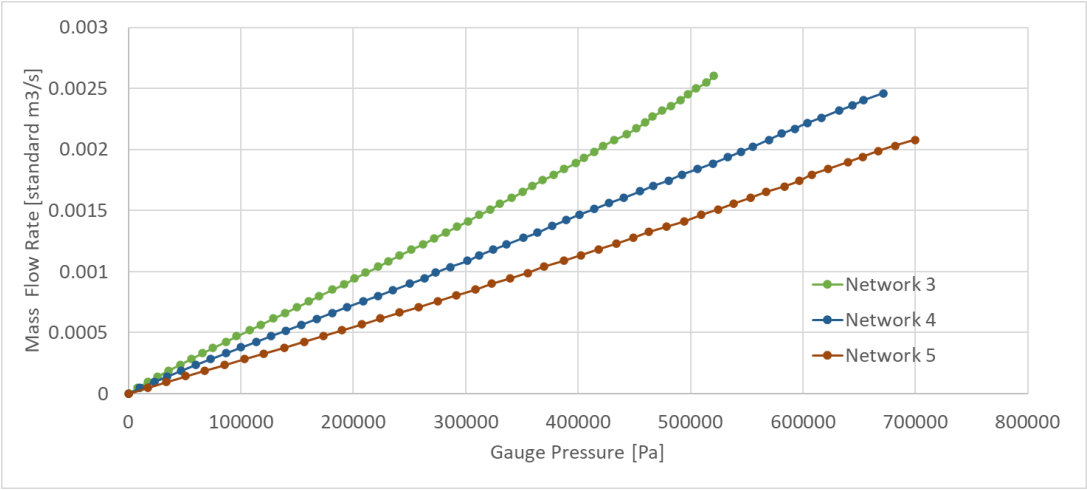

Figure 3.5 Comparison of the mass flow rates of the 3 networks shown in Figure 3.4 at high pressures 0-700000 Pa

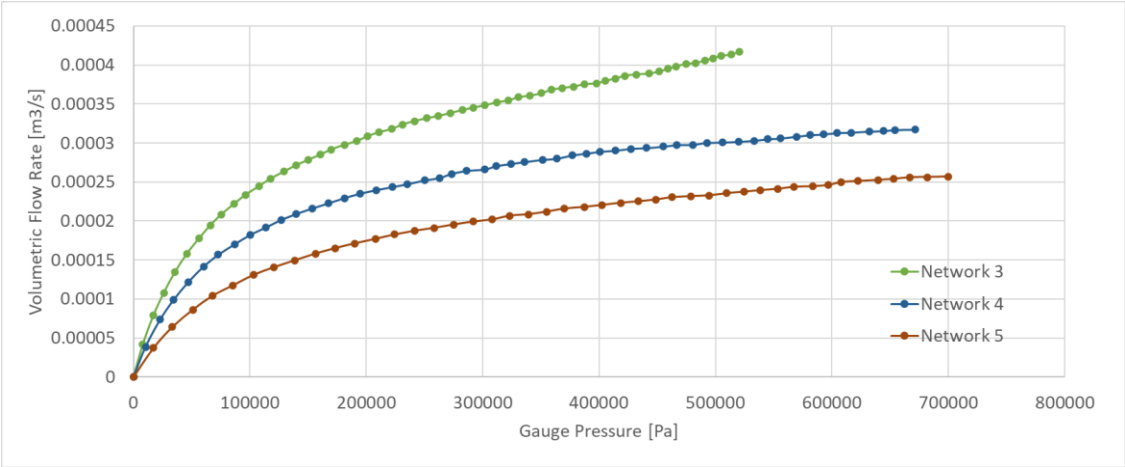

Figure 3.6 Comparison of the volumetric flow rates of the 3 networks shown in Figure 3.4 at high pressures 0-700000 Pa

3.1.2 Field Testing

Field testing was conducted in 10 locations in the state of California, out of which 9 were residential single-family houses and 1 was a commercial facility. Both new and old housing were included in the testing; the age of the buildings ranged from 1912 to 2008.

Our procedure and apparatus were refined and developed as we conducted more tests. Initially the apparatus only contained sensors to measure the flow and the pressure, but later, sensors were added to measure gas temperature, air temperature and barometric pressure. Temperature data was also acquired from the nearest weather station to compare with the measured air temperature trends.

It was observed that the leakage in 8 out of 10 locations tested were below the detection limit. In the 2 locations where a leakage was detected, the flexible lines were identified as a potential source of leakage. The author was also able to isolate and identify a leak in an old-style shutoff valve. Table 3.1 presents a summary of the results from the field testing.

Location Number	Test Date	Application	Appliances	Measured Leakage with Flexible Piping (Steady State) [standard mL/day/Pa]	Measured Leakage without Flexible Piping (Steady State) [standard mL/day/Pa]	Leakage with Flexible Piping Calculated from Pressure Decay and Est Volume [standard mL/day/Pa]	Geometric Estimate Pipe Volume [m^3]	Calculated Pipe Volume from Steady State and Decay [m^3]	Year of Const	Flexible Piping Leakage [standard mL/day/Pa]	Notes
1	1/29/2021	Single Family Residence (Oakland)	6	Not Available	11.2	14.5	0.0228	0.0287	1912	Not Available	
1	7/8/2021	Single Family Residence (Oakland)	6	23.2	22.4	16.2	0.0228	0.0314	1912	0.8	for 3 Flex pipes
2	4/8/2021	University Exterior HVAC Supply (Davis)	3	Not Applicable	below detection limit	below detection limit	0.0047	below detection limit	Not Available	below detection limit	
3	5/7/2021	Single Family Residence (Davis)	5	1.42	0.257	0.173	0.0060	0.0088	1978	1.163	for 4 Flex pipes
4	5/19/2021	Single Family Residence (Sacramento)	4	below detection limit	below detection limit	below detection limit	0.0055	below detection limit	2008	below detection limit	
5	6/9/2021	Single Family Residence (Woodland)	3	below detection limit	below detection limit	below detection limit	0.0116	below detection limit	2006	below detection limit	
6	6/22/2021	Single Family Residence (Davis)	3	below detection limit	below detection limit	below detection limit	0.0028	below detection limit	1946	below detection limit	
7	7/16/2021	Single Family Residence (Sacramento)	2	below detection limit	below detection limit	below detection limit	0.0092	below detection limit	1965	below detection limit	
8	7/26/2021	Single Family Residence (Sacramento)	5	below detection limit	below detection limit	below detection limit	0.0275	below detection limit	2005	below detection limit	
9	8/5/2021	Single Family Residence (Sacramento)	1	below detection limit	below detection limit	below detection limit	0.0024	below detection limit	1955	below detection limit	
10	8/19/2021	Commercial Facility (San Ramon)	1	below detection limit	below detection limit	below detection limit	0.6563	below detection limit	1985	below detection limit	

Table 3.1 Summary of Results from Field testing

3.1.2.1 Location 1

Year Of Construction:	1912
Application	Single Family Residence
Location	Oakland
No Of Appliances	6

Table 3.2 Location 1 - Details

Test 1:

Date of Testing	1/29/2021
Measured Leakage with Flexible Piping (Steady State) [standard mL/day/Pa]	*Not Available*
Measured Leakage without Flexible Piping (Steady State) [standard mL/day/Pa]	11.2
Measured Leakage for entire system (Pressure Decay) [standard mL/day/Pa]	14.5
Geometrically Estimated Pipe Volume [m^3]	0.0228
Calculated Pipe Volume from Steady State and Decay [m^3]	0.0287

Table 3.3 Location 1 – Leakage Measurement Data (Test 1)

Test 2:

Date of Testing	7/8/2021
Measured Leakage with Flexible Piping (Steady State) [standard mL/day/Pa]	23.2
Measured Leakage without Flexible Piping (Steady State) [standard mL/day/Pa]	22.4
Measured Leakage for entire system (Pressure Decay) [standard mL/day/Pa]	16.2
Geometrically Estimated Pipe Volume [m^3]	0.0228
Calculated Pipe Volume from Steady State and Decay [m^3]	0.0314

Table 3.4 Location 1 – Leakage Measurement Data (Test 2)

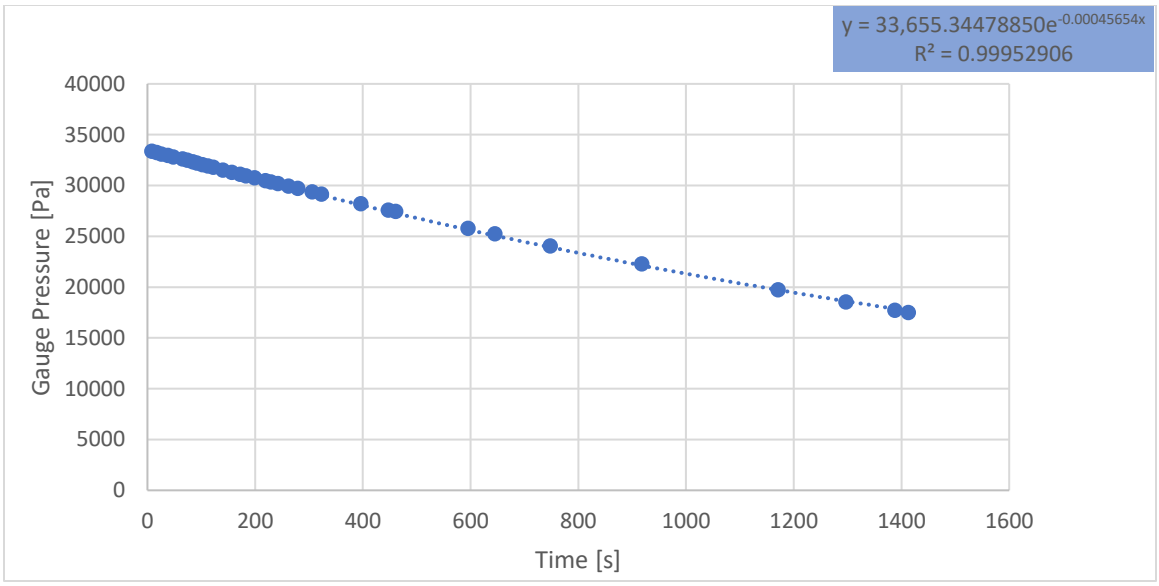

Figure 3.7 Location 1 (Test 1) Pressure Decay of entire system (including the flexible piping)

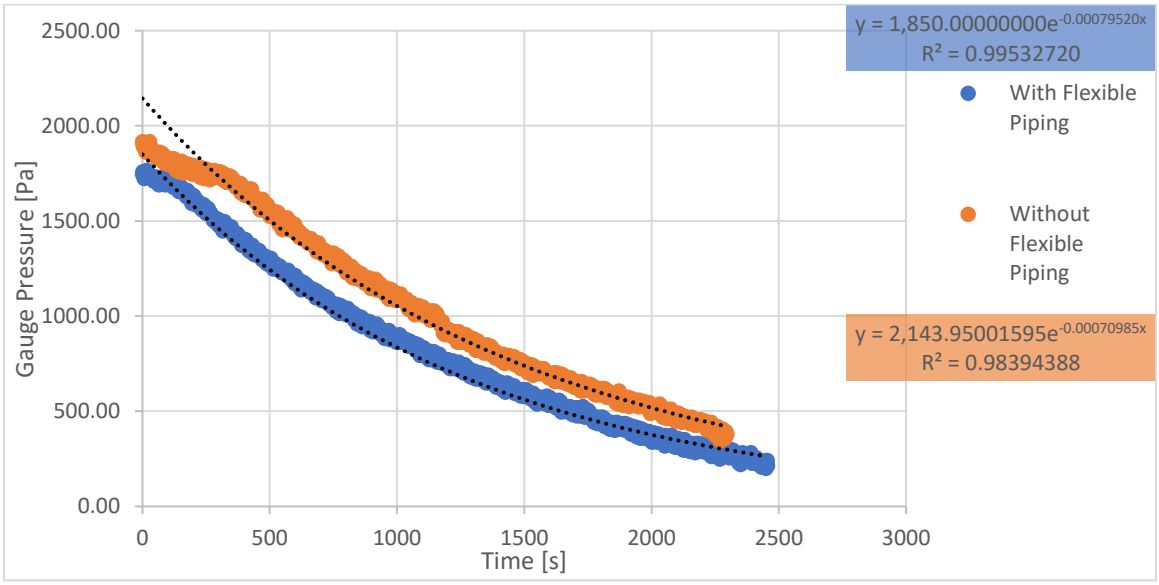

Figure 3.8 Location 1 (Test 2) Pressure Decay of entire system

Location 1 was a three-storied single-family residence constructed in 1912 and had 6 appliances connected to the gas network. This included a stove & oven unit, two furnaces, a water heater, a dryer and a barbeque. The author estimated the total volume of the network to be around 0.023 m^3.

In Test 1, the author measured a discernible pressure decay which was conclusive evidence that there was leakage in the system. From the steady state leak test that was subsequently conducted, the author measured a leakage rate of 14.5 $standard\ mL/day/Pa$. In comparison, the leakage rate calculated from the estimated volume of the gas network and the pressure decay data was 11.2 $standard\ mL/day/Pa$. The author also estimated the volume of the gas network from the steady state leak rate and the pressure decay data (Figure 3.3); this was calculated to be 0.0314 m^3. The error in the leakage rate estimation was about 23% while the error in calculating the volume was about 37%. This error is suspected to be a combination of the effect of the following two assumptions in the process of estimation:

- Uncertainty in measuring the volume of the gas system: our estimate was based on the diameters of the pipe in the exposed locations and a rough assumption of the how the pipes run through the walls.
- Uncertainty in the pressure decay fit to an exponential trendline which might not always return a perfectly fitting trendline equation.

The author suspected that there could be some inherent leakage in the apparatus that was used in Test 1 and decided to carry out another set of tests to validate the leakage measured in Test 1. The only difference between Test 1 and Test 2 was that shutoff valve of the barbeque oven was closed for the entire experiment in Test 2. Thus, the flexible piping of the barbeque oven was not included in the results from Test 2. Another point to be noted was that the two tests were conducted almost 6 months apart. The results were surprising- the leakage rate from Test 2 (22.4 $standard\ mL/day/Pa$) was almost twice that of the rate measured in Test 1 (11.2 $standard\ mL/day/Pa$) when the flexible lines were omitted from the testing. The two leak rates obtained in Test 2, with (23.2 $standard\ mL/day/Pa$) and without

(22.4 $standard\ mL/day/Pa$) the flexible piping were comparable, indicating that most of the leakage was from the non-flexible part of the system. The only possibility for the measured leakage to almost double in a span of 6 months was if some new leak had been created. Soap solution was sprayed around some exposed piping to identify any obvious leaks. The author were able to locate a leak in a shutoff valve as shown in Figure 3.5.

Figure 3.9 A leaky valve identified at Location 1

3.1.2.2 Location 2

Year Of Construction:	Not Available
Application	University Exterior HVAC
Location	Davis
Date Of Testing	4/8/2021
No Of Appliances	*3*
Measured Leakage with Flexible Piping (Steady State) [standard mL/day/Pa]	*Not Applicable*
Measured Leakage without Flexible Piping (Steady State) [standard mL/day/Pa]	*Below Detection Limit*
Measured Leakage for entire system (Pressure Decay) [standard mL/day/Pa]	*Below Detection Limit*
Geometrically Estimated Pipe Volume [m^3]	*0.0047*
Calculated Pipe Volume from Steady State and Decay [m^3]	*Below Detection Limit*

Table 3.5 Location 2 – Leakage Measurement Data

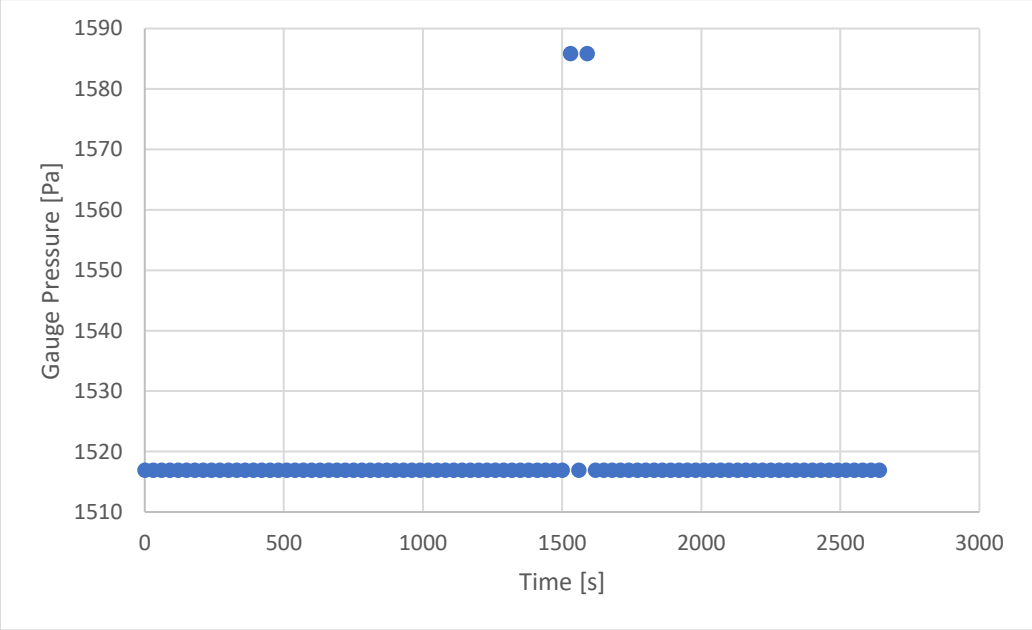

Figure 3.10 Location 2 – Pressure Decay of entire system

The 2nd location to be tested for leakage was a network consisting of 3 external HVAC units connected to each other outside a building at UC Davis. For the entire duration of the test, we did

not record any decay in the system gauge pressure. Thus, the leakage of this system was determined to be below the level of detection permissible with our apparatus (Figure 3.6).

3.1.2.3 Location 3

Year Of Construction:	1978
Application	Single Family Residence
Location	Davis
Date Of Testing	5/8/2021
No Of Appliances	5
Measured Leakage with Flexible Piping (Steady State) [standard mL/day/Pa]	1.42
Measured Leakage without Flexible Piping (Steady State) [standard mL/day/Pa]	0.257
Measured Leakage for entire system (Pressure Decay) [standard mL/day/Pa]	0.173
Geometrically Estimated Pipe Volume [m^3]	*0.0060*
Calculated Pipe Volume from Steady State and Decay [m^3]	*0.0088*

Table 3.6 Location 3 – Leakage Measurement Data

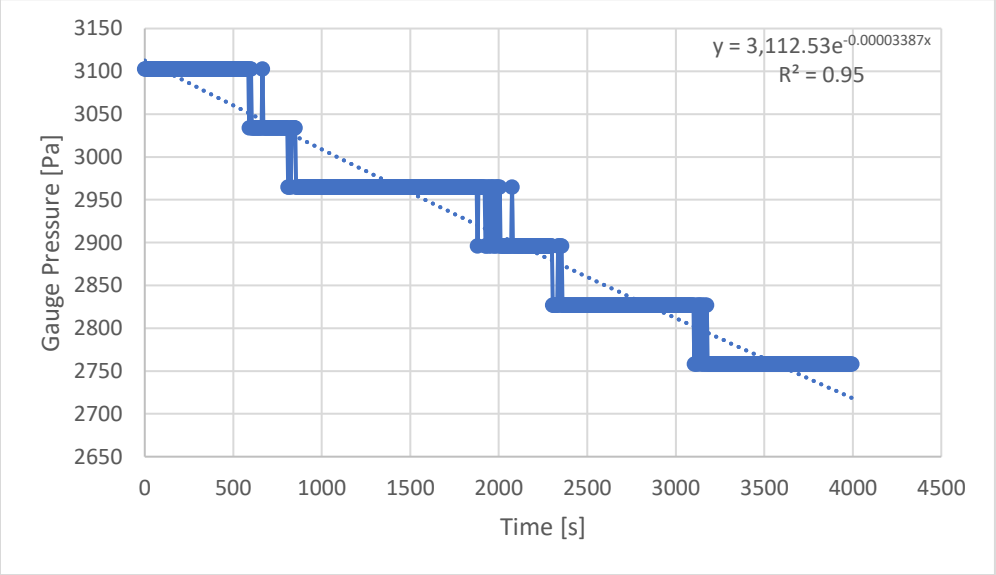

Figure 3.11 Location 3 – Pressure Decay of entire system (without flexible piping)

Location 3 was a single-storied single-family residence constructed in 1978 and located in Davis, California. It had five appliances including a stove, a water heater, a furnace, a drier and a fireplace. It is to be noted that flexible piping was used as a part of the leak measurement apparatus to connect to the gas network and was permanently included in all the experiments

conducted. When referring to flexible piping in the below description, the author means the flexible piping that was originally present in the system and not the one introduced by the author to connect to the system. The total volume of the network was estimated to be 0.0060 m^3.

A decay in pressure confirmed the presence of a leak in the system without including the flexible lines. The calculated leakage corresponding to this decay and the estimated system volume were roughly 0.173 $standard\ mL/day/Pa$. On the other hand, the leakage measured from the steady state leak testing without including the flexible piping was 0.257 $standard\ mL/day/Pa$, which is a difference of about 32%. When including the flexible piping, the steady-state leakage value increased to 1.42 $standard\ mL/day/Pa$. The pipe volume calculated from the steady state leakage and the pressure decay data was about 0.0088 m^3.

An important observation to make from the above results is that the flexible lines are responsible for 80% of the leakage observed in the above gas network.

3.1.2.4 Location 4

Year Of Construction:	2008
Application	Single Family Residence
Location	Sacramento
Date Of Testing	5/19/2021
No Of Appliances	4
Measured Leakage with Flexible Piping (Steady State) [standard mL/day/Pa]	*Below Detection Limit*
Measured Leakage without Flexible Piping (Steady State) [standard mL/day/Pa]	*Below Detection Limit*
Measured Leakage for entire system (Pressure Decay) [standard mL/day/Pa]	*Below Detection Limit*
Geometrically Estimated Pipe Volume [m^3]	*0.0055*
Calculated Pipe Volume from Steady State and Decay [m^3]	*Below Detection Limit*

Table 3.7 Location 4 – Leakage Measurement Data

Location 4 was a relatively newer construction located in Sacramento. Built in 2008, this single-family residence had 4 appliances connected to its gas network which constituted a total volume of 0.0055 m^3.

Figure 3.8 indicates the pressure profiles of the system when the flexible lines were included. Table 3.8 explains the observations of the graph It is to be noted that no data could be obtained from nearby stations for outside air temperature data for the day the test was conducted. The pressure profile showed 3 different trends when tested: rise, decrease and stability. As a result, it was difficult for the author to ascertain the presence of any leak in the system. The leakage was noted to be below the detection limit. Although the author suspects a potential influence of the outside air temperature on the gas temperature and hence the pressure, there is no atmospheric temperature data to refute or confirm this claim. While the gas temperature data measured by the flow sensor is available, the author suspects that the temperature could vary throughout the network, and the temperature measured at one location is not representative of the whole.

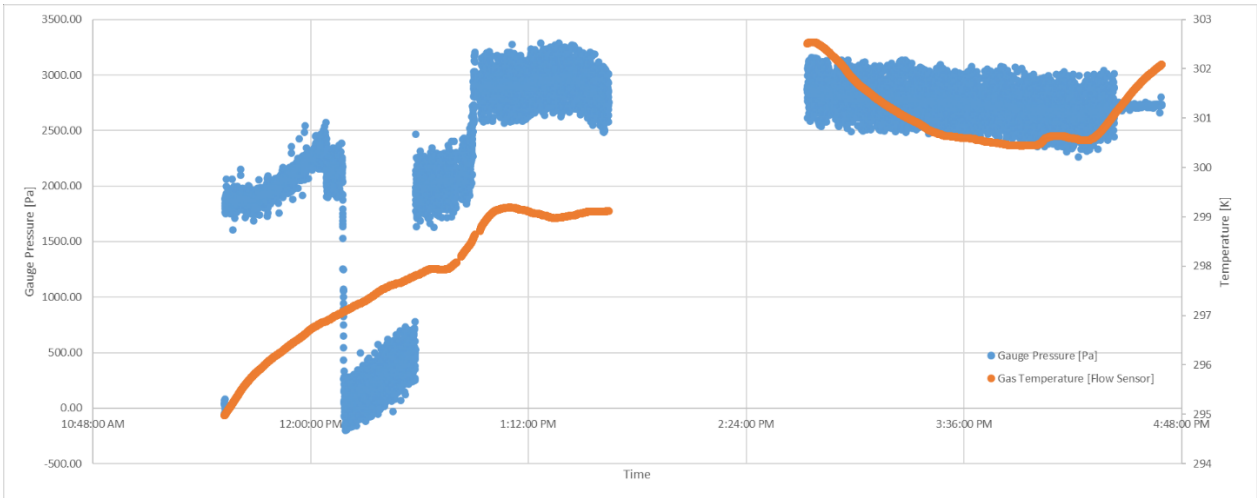

Figure 3.12 Location 4 – Pressure profile

Time	***Experiment***	***Observation***	***Explanation***
11:30 AM – 12:10 PM	Observation of the pressure profile	Rise in pressure	Potential influence of outside air temperature on gas temperature and hence gas pressure (no temperature data to validate)
12:10 PM – 12:35 PM	Observation of pressure profile after exhausting all the gas from the system	Rise in pressure	Potential influence of outside air temperature on gas temperature and hence gas pressure (no temperature data to validate)
12:35 PM – 1:32 PM	Observation of pressure profile after refilling the gas in the system by momentarily turning on the main valve and then injecting compressed air to increase system pressure	Pressure rises slowly before the compressed air was injected. After the compressed air was injected, the pressure profile remained flat and showed a drop after 1:25 PM	Potential influence of outside air temperature on gas temperature and hence gas pressure (no temperature data to validate)

2:45 PM – 4:45 PM	Observation of pressure profile	Slow decay in pressure	Although a decay is observed, it cannot be ascertained that a leak exists in the system because the two previous observations of the pressure profile indicated two different trends – an increase in pressure as well as a steady pressure profile. So, this decay could potentially be attributed to the drop in gas temperature. No atmospheric temperature data was available to confirm this claim.

Table 3.8 Location 4 – Experiments, observations, and inferences

3.1.2.5 Location 5

Year Of Construction:	2006
Application	Single Family Residence
Location	Woodland
Date Of Testing	6/9/2021
No Of Appliances	3
Measured Leakage with Flexible Piping (Steady State) [standard mL/day/Pa]	*Below Detection Limit*
Measured Leakage without Flexible Piping (Steady State) [standard mL/day/Pa]	*Below Detection Limit*
Measured Leakage for entire system (Pressure Decay) [standard mL/day/Pa]	*Below Detection Limit*
Geometrically Estimated Pipe Volume [m^3]	*0.0116*
Calculated Pipe Volume from Steady State and Decay [m^3]	*Below Detection Limit*

Table 3.9 Location 5 – Leakage Measurement Data

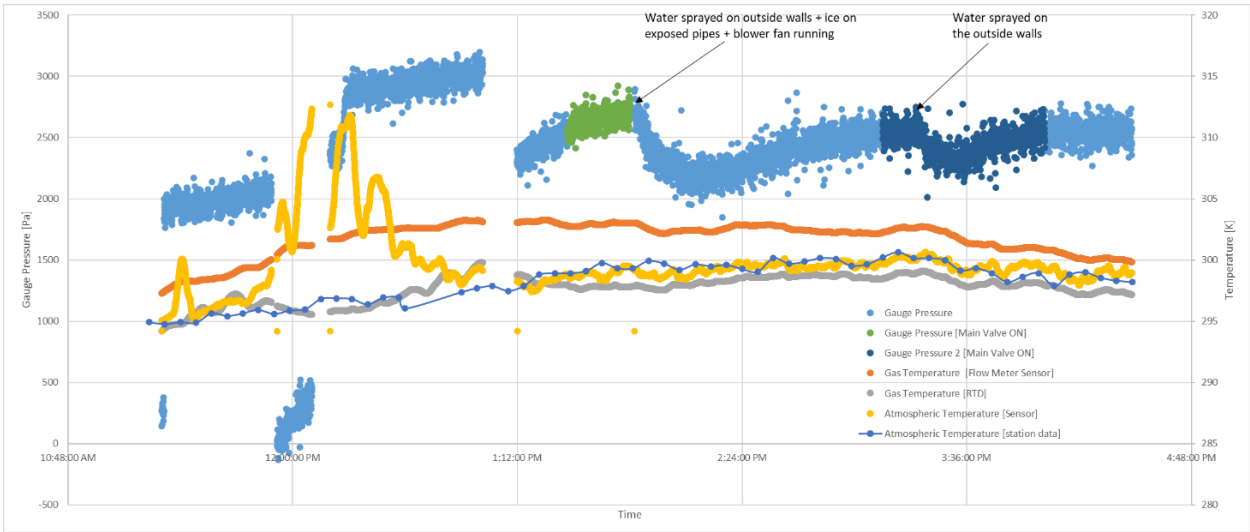

Figure 3.13 Location 5 – Pressure profile

Location 5 is a single-family residence constructed in 2006 with 3 appliances connected to the gas network. The total volume of the pipe network was estimated to be about 0.0116 m^3.

Figure 3.9 indicates the pressure profile of the gas in the system over the course of the experiment. Table 3.10 elucidates on the trends observed in Figure 3.9 and provides possible explanations for the observations. Application of cold water and ice on the exposed piping showed an instant decrease in gas pressure as a result of a temperature drop. An important conclusion from the above test is that the temperature of the atmosphere greatly influences the gas pressure. The atmospheric temperature data acquired from a nearby station validated this observation. Due to the high degree of dependence of gas pressure on the atmospheric temperature, it was difficult to ascertain the presence of a leakage in the system. Thus, the leakage was noted to be below the detection limit.

Time	***Experiment***	***Observation***	***Explanation***
11:20 AM -11:55 AM	Observation of Pressure profile	Rise in pressure	Rise in atmospheric temperature cases a rise in gas temperature and hence causes a rise gas pressure (Refer to increasing atmospheric temperature data)
11:55 AM – 12:05 PM	Observation of Pressure profile after exhausting all the natural gas in the system	Rise in pressure	Rise in atmospheric temperature cases a rise in gas temperature and hence causes a rise gas pressure (Refer to increasing atmospheric temperature data)
12:05 PM – 1 PM	Observation of pressure profile after refilling natural gas in the system by momentarily turning ON main valve and then injecting compressed air to further increase the pressure above the normal operating pressure	Rise in pressure	Rise in atmospheric temperature cases a rise in gas temperature and hence causes a rise gas pressure (Refer to increasing atmospheric temperature data)
1:12 PM – 1:28 PM	Before commencing the test, the system was completely exhausted of all the gas and	Rise in pressure	Rise in atmospheric temperature cases a rise in gas temperature and hence

	then main valve was momentarily turned ON to refill the system		causes a rise gas pressure (Refer to increasing atmospheric temperature data)
1:28 PM – 1:40 PM	Observation of pressure profile with main valve turned ON	Rise in pressure. The slope of pressure rise keeps decreasing with time and the pressure seems like it is approaching a stable value	When main valve was turned ON, steady atmospheric temperature values resulted in stable gas temperature values and thereby stable gas pressure values (Refer to steady atmospheric temperature data)
1:40 PM – 3:00 PM	Main valve turned OFF and water sprayed on outside walls, ice kept on exposed piping and blower fan turned inside the house to cool	Sudden drop in pressure followed by recovery	Pressure drop due to immediate drop in gas temperature as cold water was sprayed on the exposed piping. The temperature then slowly increased because of the influence of atmospheric temperature on the gas temperature – the hotter air outside was heating the cold gas inside the pipe and this caused the gas pressure to also recover
3:00 PM – 4:04 PM	Observation of pressure profile with main valve ON ; cold water sprayed on outside walls at 3:22 PM	As soon as the main valve was ON, the pressure started stabilizing as indicated by a near-linear slope. When cold water was sprayed the pressure dropped immediately and recovered quickly; the pressure soon approached	When main valve was turned ON, steady atmospheric temperature values resulted in stable gas temperature values and thereby stable gas pressure values (Refer to steady atmospheric temperature data). Pressure drop due to immediate drop in gas temperature as cold water was sprayed. The temperature then slowly increased because of the influence of outside air temperature and caused a rise in gas pressure

		stabilization	
4:04 PM – 4:30 PM	Observation of pressure profile with main valve OFF	Stable pressure	When main valve was turned OFF, steady atmospheric temperature values resulted in stable gas temperature values and thereby stable gas pressure values (Refer to steady atmospheric temperature data).

Table 3.10 Location 5 – Experiments, observations, and inferences

3.1.2.6 Location 6

Year Of Construction:	1940
Application	Single Family Residence
Location	Davis
Date Of Testing	6/22/2021
No Of Appliances	3
Measured Leakage with Flexible Piping (Steady State) [standard mL/day/Pa]	*Below Detection Limit*
Measured Leakage without Flexible Piping (Steady State) [standard mL/day/Pa]	*Below Detection Limit*
Measured Leakage for entire system (Pressure Decay) [standard mL/day/Pa]	*Below Detection Limit*
Geometrically Estimated Pipe Volume [m^3]	*0.0028*
Calculated Pipe Volume from Steady State and Decay [m^3]	*Below Detection Limit*

Table 3.11 Location 6 – Leakage Measurement Data

Location 6 was a single-family residence constructed in 1940 with a total gas system volume of 0.0028 m^3. A total of 3 appliances were connected to the gas system.

Figure 3.10 indicates the pressure profile of the gas in the system over the course of the experiment and Table 3.12 provides possible explanations for the observations. It is to be noted that when testing the effect of temperature on the gas system in Location 5 cold water was sprayed on the walls and a blower fan was turned on to cool the house, in addition to ice applied on exposed piping, all of which together contributed to the decrease in the temperature of the gas in the network and the pressure. But in the case of Location 6, there was only ice that was applied over the little exposed piping, which was a small volume when compared to the entire system. Thus, the thermal mass of the ice applied was not enough to cause a change in the temperature of the gas. The pressure profile (which showed no drop in pressure) also suggested that this was not enough to overcome the increase in gas temperature due to the increase in outside atmospheric temperature. Overall, the pressure profile data (Figure 3.10) does not indicate the presence of any leaks in the system.

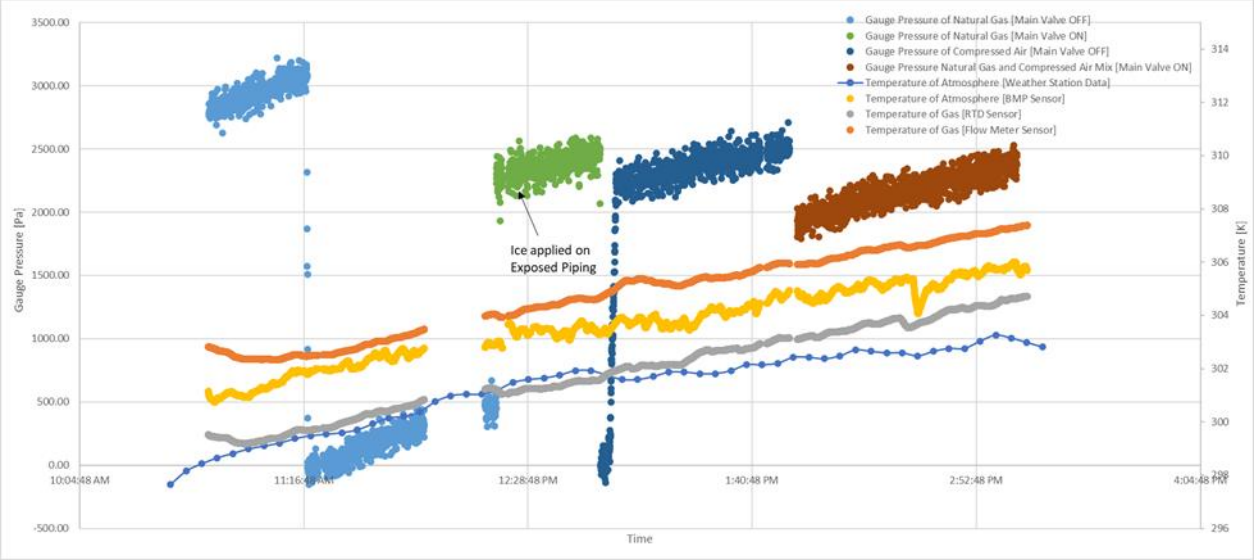

Figure 3.14 Location 6 – Pressure and temperature profile

Time	***Experiment***	***Observation***	***Inference***
10:45 AM – 11:16 AM	Observing pressure profile with main valve OFF	Rise in pressure	Rise in atmospheric temperature cases a rise in gas temperature and hence causes a rise gas pressure (Refer to increasing atmospheric temperature data)
11:16 AM – 12:15 PM	Gas exhausted from system and pressure profile observed with main valve OFF	Pressure rises until 11:55 AM when experiment temporarily paused	Rise in atmospheric temperature cases a rise in gas temperature and hence causes a rise gas pressure (Refer to increasing atmospheric temperature data)
12:15 PM – 12:45 PM	Observation of pressure profile (Main valve was turned ON at about 12:18 PM). Ice applied on exposed piping at about 12:25 PM	Pressure rises. No effect due to ice since the available exposed piping was very minimal and there was only	Rise in atmospheric temperature cases a rise in gas temperature and hence causes a rise gas pressure (Refer to increasing atmospheric temperature data) Effect of increase in gas

		little ice applied	temperature due to atmospheric temperature greater than effect of temperature reduction due to ice application.
12:45 PM – 1:50 PM	Gas exhausted from system and main valve turned OFF. Compressed air injected into the system and pressure profile observed	Rise in pressure	Rise in atmospheric temperature cases a rise in gas temperature and hence causes a rise gas pressure (Refer to increasing atmospheric temperature data)
1:50 PM – 3:00 PM	Gas slightly exhausted and main valve turned ON to observe pressure profile	Rise in pressure	Rise in atmospheric temperature cases a rise in gas temperature and hence causes a rise gas pressure (Refer to increasing atmospheric temperature data)

Table 3.12 Location 6 – Experiments, observations, and inferences

3.1.2.7 Location 7

Year Of Construction:	1965
Application	Single Family Residence
Location	Sacramento
Date Of Testing	7/16/2021
No Of Appliances	2
Measured Leakage with Flexible Piping (Steady State) [standard mL/day/Pa]	*Below Detection Limit*
Measured Leakage without Flexible Piping (Steady State) [standard mL/day/Pa]	*Below Detection Limit*
Measured Leakage for entire system (Pressure Decay) [standard mL/day/Pa]	*Below Detection Limit*
Geometrically Estimated Pipe Volume [m3]	*0.0092*
Calculated Pipe Volume from Steady State and Decay [m3]	*Below Detection Limit*

Table 3.13 Location 7 – Leakage Measurement Data

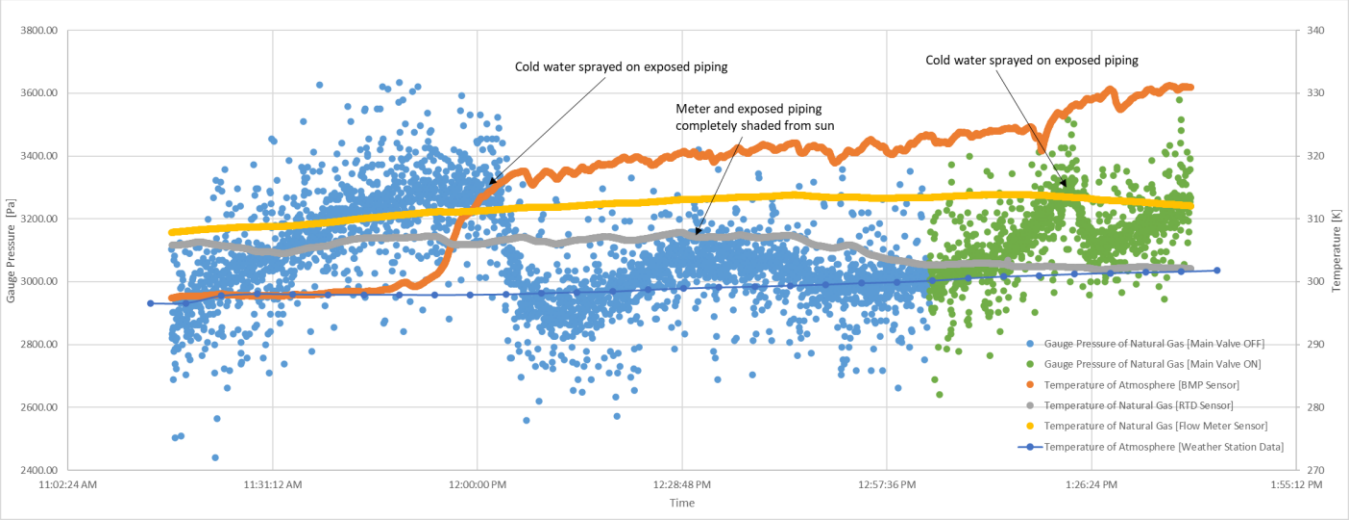

Figure 3.15 Location 7 – Pressure profile

Location 7 was a single-family residence built in 1965 with 2 gas-fired appliances which included a heater and a furnace. The entire volume of the gas system amounted to about 0.0092 m^3.

From the initial observation of pressure increase, it seemed apparent that the rise in atmospheric temperature influenced the pressure and caused it to rise. But the observation between 12:15 PM

and 1:15 PM potentially countered this argument since we saw both an increase and a decrease in pressure while the pressure was recovering after being lowered due to the application of cold-water. While the rise in pressure can be attributed to the increase in gas temperature as it was recovering from the temperature drop, the decrease at 12:40 PM makes the author suspect a leak in the system. Between 12:40 PM and 1 PM, the shade cover on the exposed pipe section keeps increasing until the pipe is fully covered at 1 PM (Figure 3.12). Following this, the author observed a steady increase as noted previously. This could mean that while the shade was slowly covering the exposed piping the decrease in the gas temperature was counter-acting the increase in gas temperature due to the atmospheric temperature rise. The drop in temperature because of the cooling effect of the shade cover dominated until a while after the piping was completely shaded from the sun, after which the pressure of the gas can be observed to increase again. (Figure 3.11). Refer to Table 3.14 for more information on the pressure profile observations and possible explanations.

Leakage in Location 7 was thus determined to below the detection limit since the pressure profile was heavily influenced by the changing atmospheric temperature.

Time	***Experiment***	***Observation***	***Inference***
11:15 AM – 12:00 PM	Observation of pressure profile	Steady rise in pressure until 12 PM	Rise in atmospheric temperature cases a rise in gas temperature and hence causes a rise gas pressure (Refer to increasing atmospheric temperature data)
12:00 PM – 1:15 PM	Cold water sprayed on exposed piping	Pressure drops until 12:10 PM and starts to recover, attained a peak at 12:40 PM,	Pressure drop due to immediate drop in gas temperature as cold water was sprayed on the exposed piping. The temperature then slowly increased

		drops again until 1 PM and rises again until 1:15 PM	because of the influence of atmospheric temperature on the gas temperature – the hotter air outside was heating the cold gas inside the pipe and this caused the gas pressure to also recover. But the changing shade cover on the exposed piping due to the change in the position of the sun interfered with the recovery. This created a cooling effect that interfered with the recovery (Figure 4.28)
1:15 PM – 1:25 PM	Main shutoff valve turned ON	Slope of pressure rise increases to a value greater than the slope between 1 PM and 1:15 PM.	The gas upstream could have been hotter than the gas inside the system and as a result the temperature of the gas increases at a steeper rate and hence the pressure also increases at a steeper rate.
1:25 PM – 1:40 PM	Cold water sprayed on exposed piping	Pressure dropped until 1:30 PM and started steady rising until the experiment concluded at 1:40 PM	Pressure drop due to immediate drop in gas temperature as cold water was sprayed.

Table 3.14 Location 7 – Experiments, observations, and inferences

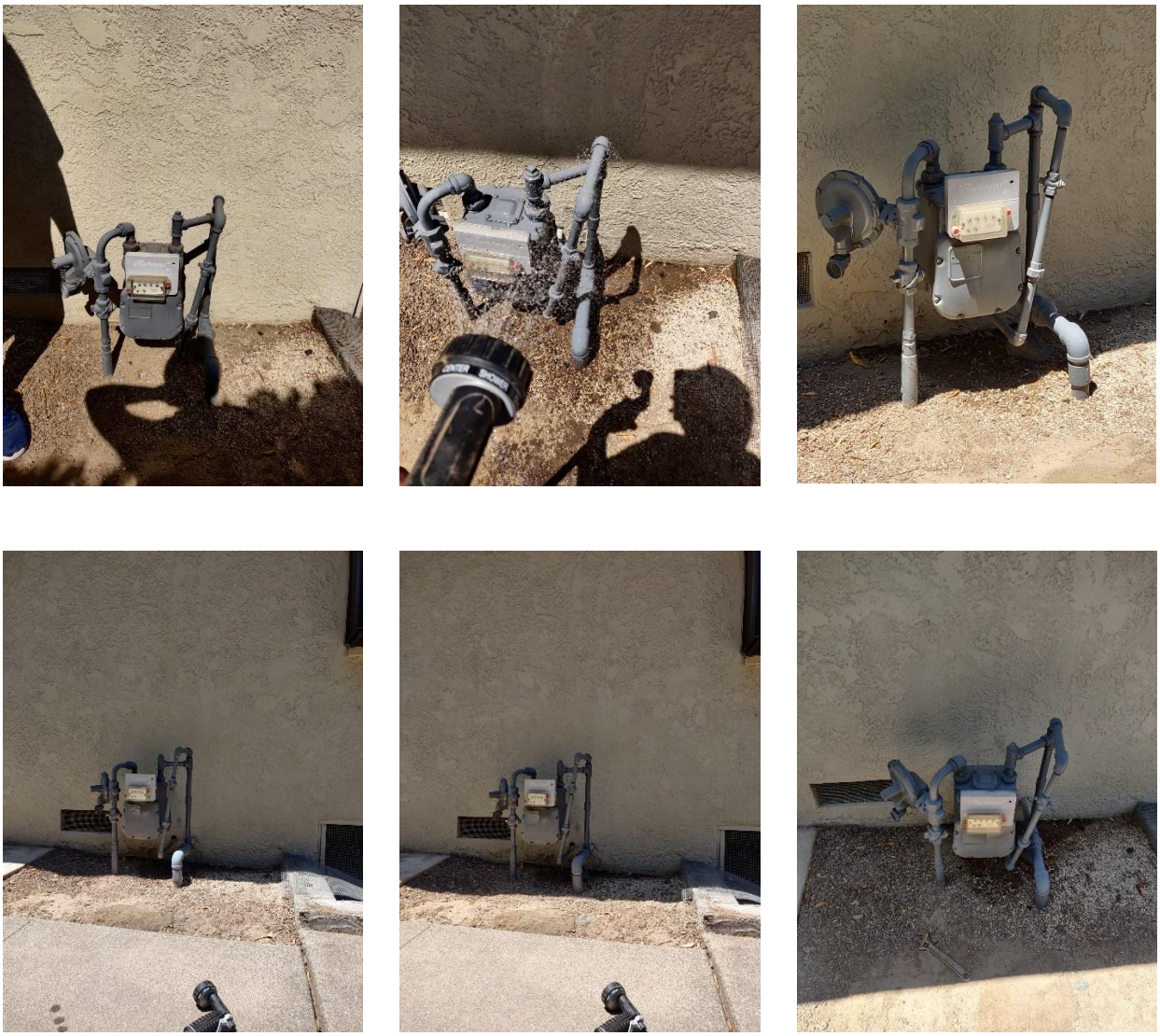

Figure 3.16 Change of shade cover on the exposed pipe sections with time.

3.1.2.8 Location 8

Year Of Construction:	2005
Application	Single Family Residence
Location	Sacramento
Date Of Testing	7/26/2021
No Of Appliances	5
Measured Leakage with Flexible Piping (Steady State) [standard mL/day/Pa]	*Below Detection Limit*
Measured Leakage without Flexible Piping (Steady State) [standard mL/day/Pa]	*Below Detection Limit*
Measured Leakage for entire system (Pressure Decay) [standard mL/day/Pa]	*Below Detection Limit*
Geometrically Estimated Pipe Volume [m^3]	*0.0275*
Calculated Pipe Volume from Steady State and Decay [m^3]	*Below Detection Limit*

Table 3.15 Location 8 – Leakage Measurement Data

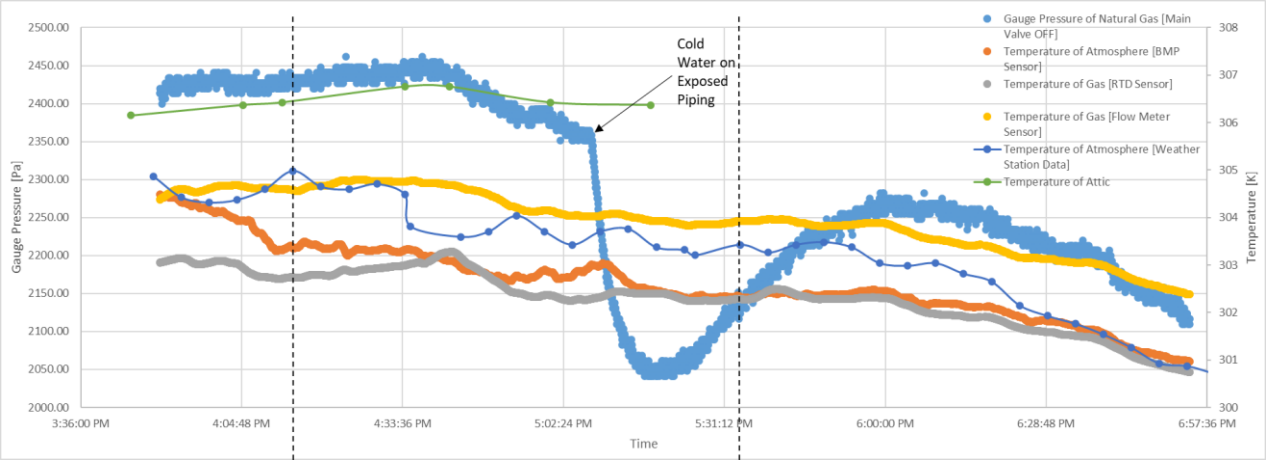

Figure 3.17 Location 8 – Pressure and temperature profile

Location 8 is also a single-family residence home located in Sacramento, CA. 5 appliances were connected to the gas supply network which had a total volume of 0.0275 m^3.

Figure 3.13 graphically indicates the profiles of pressure and temperature over the course of the experiment. Table 3.16 explains the observations and infers possible causes.

The house had a temperature sensor in the attic, and the author was able to obtain recordings of the attic temperatures over a portion of our experiment. A point of difference between this location and other locations was that we tested quite late in the evening just before the temperature attained its peak and starts to drop. Until the time the attic temperatures were recorded, the gas pressure and the attic temperature follow a similar trend. This makes the author wonder if the temperature of the attic had a large influence on the overall gas temperature and hence the gas pressure.

Based on the experiments, the overall conclusion is that any decay observed is influenced by the reduction in temperature and hence the leakage in Location 8 was deemed to be below the detection limit.

Time	***Experiment***	***Observation***	***Inference***
3:50 PM – 4:30 PM	Observation of pressure profile	Rise in pressure until 4:30 PM. Attic temperatures are seen rising during this period	Rise in attic temperature cases a rise in gas temperature and hence causes a rise gas pressure (Refer to increasing attic temperature data). Although the atmospheric temperatures are seen to drop during this period, the rise in the gas pressure indicates that the increasing attic temperature dominate over the decreasing atmospheric temperature and results in a net rise in the gas temperature and hence the gas pressure
4:30 PM – 5:05 PM	Tarpaulin sheet spread on the roof as a shield	Pressure stayed constant for about 5 minutes, before	The attic temperatures and the atmospheric temperatures are seen to drop during this period.

		it started to drop. The attic temperature starts to drop at around the same time	Both of these collectively influence the drop in gas temperature and hence the gas pressure. Spreading the tarpaulin sheet further shielded the roof from the direct heating effect of the sun and hence as a result, the drop in temperatures are suspected to be steeper than the previous scenario.
5:05 PM – 6:55 PM	Cold water sprayed on exposed piping	Pressure drops and recovers at about 5:15 PM and starts increasing until 6:15 PM before it starts dropping again.	Pressure drops due to immediate temperature drop caused by the cold water, but pressure recovers due to the heating effect of the outside air, but once it fully recovers, it starts to drop again because the outside air temperature itself is decreasing.

Table 3.16 Location 8 – Experiments, observations, and inferences

3.1.2.9 Location 9

Year Of Construction:	1955
Application	Single Family Residence
Location	Sacramento
Date Of Testing	8/05/2021
No Of Appliances	1
Measured Leakage with Flexible Piping (Steady State) [standard mL/day/Pa]	*Below Detection Limit*
Measured Leakage without Flexible Piping (Steady State) [standard mL/day/Pa]	*Below Detection Limit*
Measured Leakage for entire system (Pressure Decay) [standard mL/day/Pa]	*Below Detection Limit*
Geometrically Estimated Pipe Volume [m^3]	0.0024
Calculated Pipe Volume from Steady State and Decay [m^3]	*Below Detection Limit*

Table 3.17 Location 9 – Leakage Measurement Data

Location 9 is a single-family residence built in 1955 with 1 appliance connected to the gas network. There was another appliance previously connected to the network but currently only the piping that runs to this appliance remains a part of the network. Total volume of the gas system amounted to 0.0024 m^3.

Figure 3.14 graphically indicates the profiles of pressure and temperature over the course of the experiment. Table 3.18 explains the observations and infers possible causes.

Overall, the conclusion is that the gas network at location 9 was below the detection limit and the variation in gas pressure because of potential gas temperature fluctuations masked any potential leaks in the system.

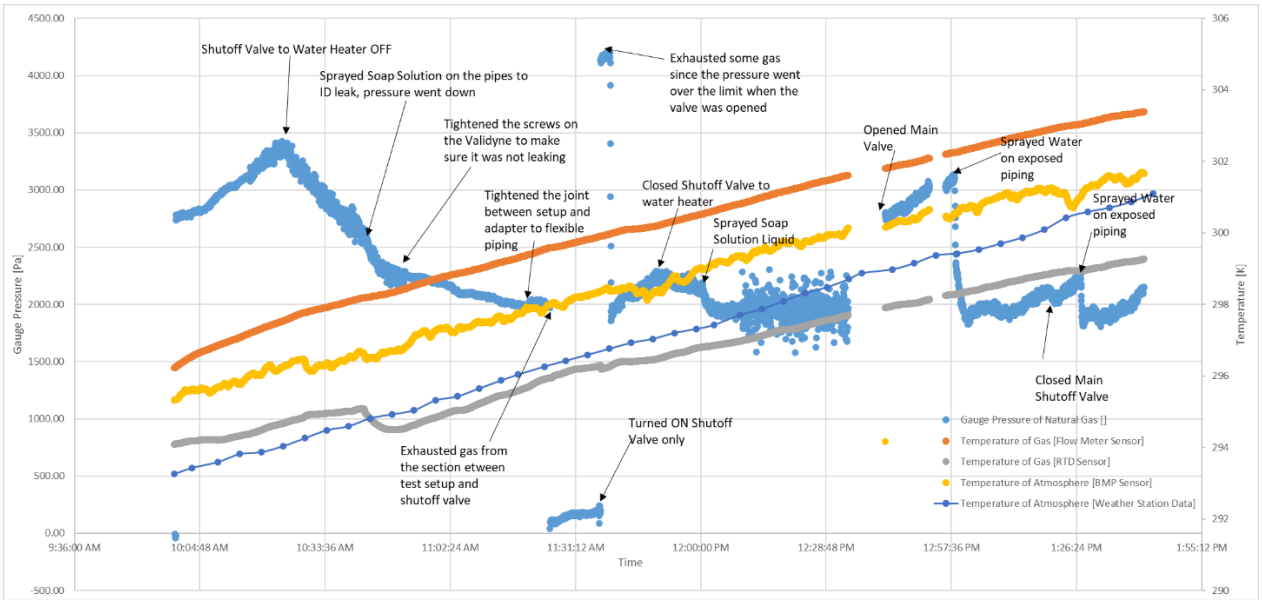

Figure 3.18 Location 9 – Pressure and temperature profile

Time	***Experiment***	***Observation***	***Inference***
10:00 AM – 10:20 AM	Observation of pressure profile of the gas	Rise in pressure	Rise in atmospheric temperature cases a rise in gas temperature and hence causes a rise gas pressure (Refer to increasing atmospheric temperature data)
10:20 AM – 10:44 AM	Closed the Shutoff Valve to the Water Heater	Drop in pressure	Potential for leak in test apparatus (not the system being tested)
10:44 AM – 10:50 AM	Sprayed liquid soap solution to identify potential leaks in test apparatus	Pressure Drop at a higher slope than previous scenario	Cold soap solution interacts with the gas to reduce its temperature and thereby reduces the gas pressure in the test apparatus
10:50 AM – 11:22 AM	Tightened the screws on the Pressure Gauge to eliminate potential cause for leakage	Reduced Slope of Pressure Drop; Reduced Fluctuation of	Eliminated potential for leakage through pressure gauge

		Pressure	
11:22 AM – 11:26 AM	Tightened the adapter that connects apparatus to flexible piping	Short increase in Pressure followed by drop	Eliminated potential for leakage through adapter that connects apparatus to flexible piping
11:26 AM – 11:39 AM	Exhausted gas from section upstream of shutoff valve to water heater	Rise in pressure	Rise in atmospheric temperature cases a rise in gas temperature and hence causes a rise gas pressure (Refer to increasing atmospheric temperature data)
11:39 AM – 11:40 AM	Turned on shutoff valve to water heater	Pressure rose to over safety limit	Since all the previous experiments were done with the Main Shutoff Valve OFF, the gas in the section between the main valve and the shutoff valve to water heater could have risen in pressure due to the rise in outside air temperature that caused the gas temperature to rise.
11:40 AM – 11:49 AM	Exhausted some gas to reduce pressure to below the safety limit	Immediate pressure drop followed by steady rise	Rise in atmospheric temperature cases a rise in gas temperature and hence causes a rise gas pressure (Refer to increasing atmospheric temperature data)
11:49 AM – 12:00 PM	Closed shutoff valve to water heater	Pressure drops, but at a lower slope compared to previous pressure drops for the same section	The temperature of the room is lower than the outside temperature. Since the test apparatus section was isolated when the shutoff valve was closed, the temperature of the gas in the system dropped in order to achieve equilibrium with the room temperature and hence the gas pressure dropped
12:00 PM – 12:33 PM	Sprayed liquid soap solution to identify potential leaks in test section	Quick pressure drop followed by constant pressure values	Spraying the soap solution helped the gas in the test apparatus section achieve equilibrium faster. Once it

		and increased fluctuation of pressure.	achieved equilibrium the temperature is expected to stay constant (since the room temperature was controlled) and as a result, the gas pressure is observed to be constant
12:40 PM – 12:57 PM	Opened shutoff valve to water heater and main shutoff valve	Rise in pressure	Rise in atmospheric temperature cases a rise in gas temperature and hence causes a rise gas pressure (Refer to increasing atmospheric temperature data)
12:57 PM – 1:22 PM	Sprayed Water on exposed piping near main shutoff valve	Pressure Drop followed by slow rise in pressure (overall pressure rise, but in a wavy manner with a maxima and minima)	Pressure drop due to immediate drop in gas temperature as cold water was sprayed on the exposed piping, followed by recovery of pressure. The pressure keeps rising afterwards because of the rise in atmospheric temperature which causes a rise in gas temperature and hence causes a rise gas pressure (Refer to increasing atmospheric temperature data)
1:22 PM – 1:27 PM	Closed main shutoff valve	Immediate Rise in pressure at a greater slope than between 12:57 PM and 1:22 PM	Rise in atmospheric temperature which causes a rise in gas temperature and hence causes a rise gas pressure (Refer to increasing atmospheric temperature data). The rise in pressure is at a greater slope because when the main shutoff valve is open, the interaction of the gas in the pipe with the atmosphere is reduced because the piping upstream of the main valve is buried underneath. When the main

			shutoff valve is closed, only the downstream piping included. Thus, the heating effect of the atmosphere on the gas is higher when the main shutoff valve is closed because a higher portion of the piping is exposed to the atmosphere and hence the effect of the atmospheric temperature on the gas is higher
1:27 PM – 1:40 PM	Sprayed water on exposed piping near main shutoff valve	Immediate Pressure drop followed by steady rise	Rise in atmospheric temperature which causes a rise in gas temperature and hence causes a rise gas pressure (Refer to increasing atmospheric temperature data).

Table 3.18 Location 9 – Experiments, observations, and inferences

3.1.2.10 Location 10

Year Of Construction:	1985
Application	Commercial Building
Location	San Ramon
Date Of Testing	8/19/2021
No Of Appliances	1
Measured Leakage with Flexible Piping (Steady State) [standard mL/day/Pa]	*Below Detection Limit*
Measured Leakage without Flexible Piping (Steady State) [standard mL/day/Pa]	*Below Detection Limit*
Measured Leakage for entire system (Pressure Decay) [standard mL/day/Pa]	*Below Detection Limit*
Geometrically Estimated Pipe Volume [m^3]	0.6563
Calculated Pipe Volume from Steady State and Decay [m^3]	*Below Detection Limit*

Table 3.19 Location 10 – Leakage Measurement Data

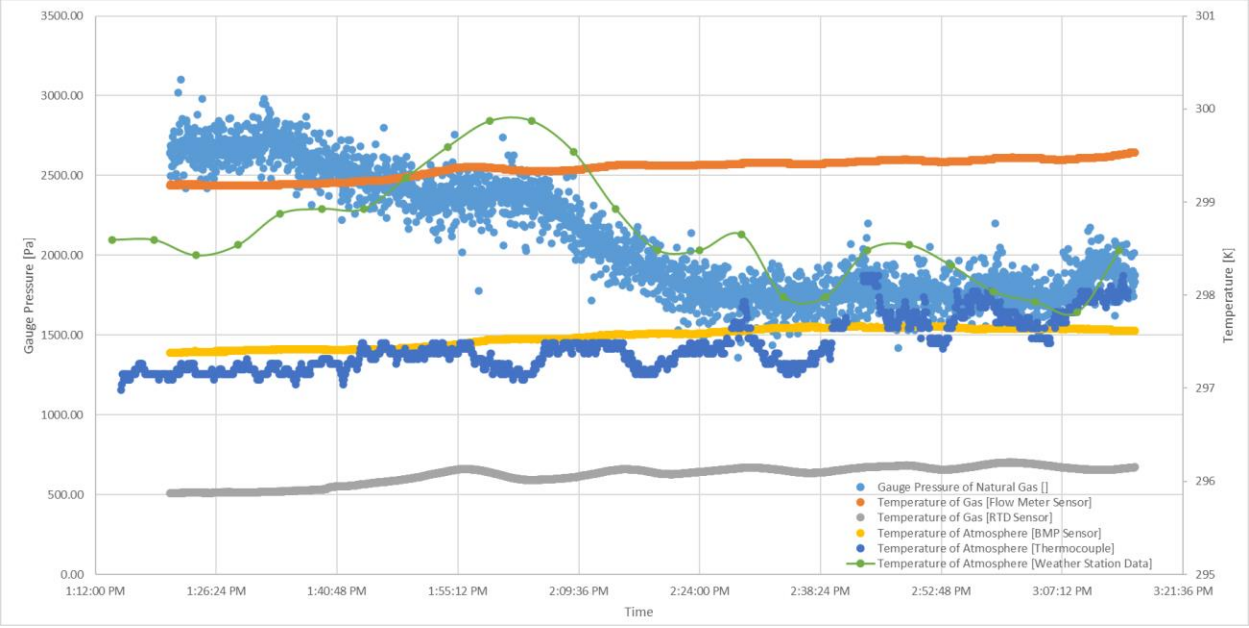

Figure 3.19 Location 10 – Pressure and temperature profile

Location 10 was a commercial facility with about 0.6563 m^3 of piping. This is the biggest facility tested in terms of volume of gas piping.

Figure 3.15 depicts the pressure and temperature profile of the gas as observed for the entire duration of the experiment. The only experiment conducted in the case of Location 10 was to observe how the pressure profile changed over the course of time. The pressure stayed constant for 15 minutes from 1:20 PM to 1:35 PM, followed by a decay until 2:24 PM. From then on, the pressure remained constant until 3:07 PM after which it started to rise again.

We suspect the possible cause of this anomalous observation is that the piping run spanned a long distance through multiple rooms and the combined temperature effects could have influenced the observed fluctuation in pressure. Since no discernible leakage was identified in this location, the leakage was noted to be below the detection limit.

3.2 LEAKAGE SEALING

3.2.1 Penetration model results

(Anand & Mcfarland, 1989)'s model was used to determine the penetration efficiency of sealant particles in a 20 m (65 ft) long horizontal pipe for different particle sizes, leak rates and pipe diameters without any pressure relief. The particle sizes analyzed ranged from 5 μm to 9 μm. Residential natural gas service lines commonly use piping of diameters of 12.7 mm, 19.1 mm, 25.4 mm (0.5 $inches$, 0.75 $inches$ or 1 $inches$) – these were the sizes that were considered for the analysis. A hundred-fold variation in the leak rate from 1.3E-08 $standard\ m^3/s$ to 1.3E-10 $standard\ m^3/s$ was also employed. For each scenario of particle size, leak rate and pipe diameter, the flow rates were varied in such a way that the range of flows encompassed both laminar and turbulent flow. The results are presented below in Figures 3.20 – 3.24.

For a 12.7 mm pipe with 5 μm particles, the max penetration efficiency drops from ~58% to 0% when the leak rate is varied from 1.3E-08 $standard\ m^3/s$ to 1.3E-10 $standard\ m^3/s$ (Figure 3.20). When the particle size is increased keeping the pipe diameter and leak rate constant, the penetration efficiency decreases (Figures 3.21). For the same particle size and leak rate, an increase in the pipe diameter results in an increase in the penetration efficiency (Figures 3.22). The issue with the above scenarios is that the pressure is high enough to cause damage to the pipe system. For a leak rate of 1.3E-08 $standard\ m^3/s$, the pressure in a 12.7 mm pipe when injected with particles of 5 μm is around 50,000 Pa at the Reynolds number corresponding to maximum penetration. This pressure is bound to increase if the leak rate in the system is lowered (Figure 3.20). The problem is that sealing without pressure relief can potentially damage the system due to the high pressures required to push the sealant particles through the system.

Similar analysis was done for scenarios with pressure relief, for different particle sizes, leak rates and pipe diameters. The general trend is similar to the observation made for the case without pressure relief. Penetration is higher for bigger pipes when the particle size is fixed; penetration is lower for bigger particles when the pipe size is fixed. A penetration efficiency of 60% is achieved when particles of 5 μm is injected into a pipe of diameter 12.7 mm. The efficiency of penetration in the same pipe drops to ~13% when the particle size is increased to 9 μm (Figure 3.23). When considering a constant particle size of 7 μm, the penetration efficiency is about 60% for a 25.4 mm pipe, 50% for a 19.1 mm pipe and 32% for a 12.7 mm pipe (Figure 3.24).

Overall, the results suggest that sealing without pressure relief can potentially damage the system due to the high pressures required to push the sealant particles through the system. The data suggests that sealing while providing pressure relief is the best way to seal the gas systems.

Pipe sizes commonly used in residential piping include 12.7 mm, 19.1 mm and 25.4 mm piping which correspond to nominal outside diameters of 21.3 mm, 26.7 mm and 33.4 mm. An important thing to consider while sealing with pressure relief is to ensure that there is sufficient pressure in the system and that the particles are able to travel across the leaks that are present throughout the system. A common rule-of-thumb is to ensure at least 30 Pa gauge pressure (check) is present at all the points in the network. With this in mind, the sealing process is designed in section 4.1 .

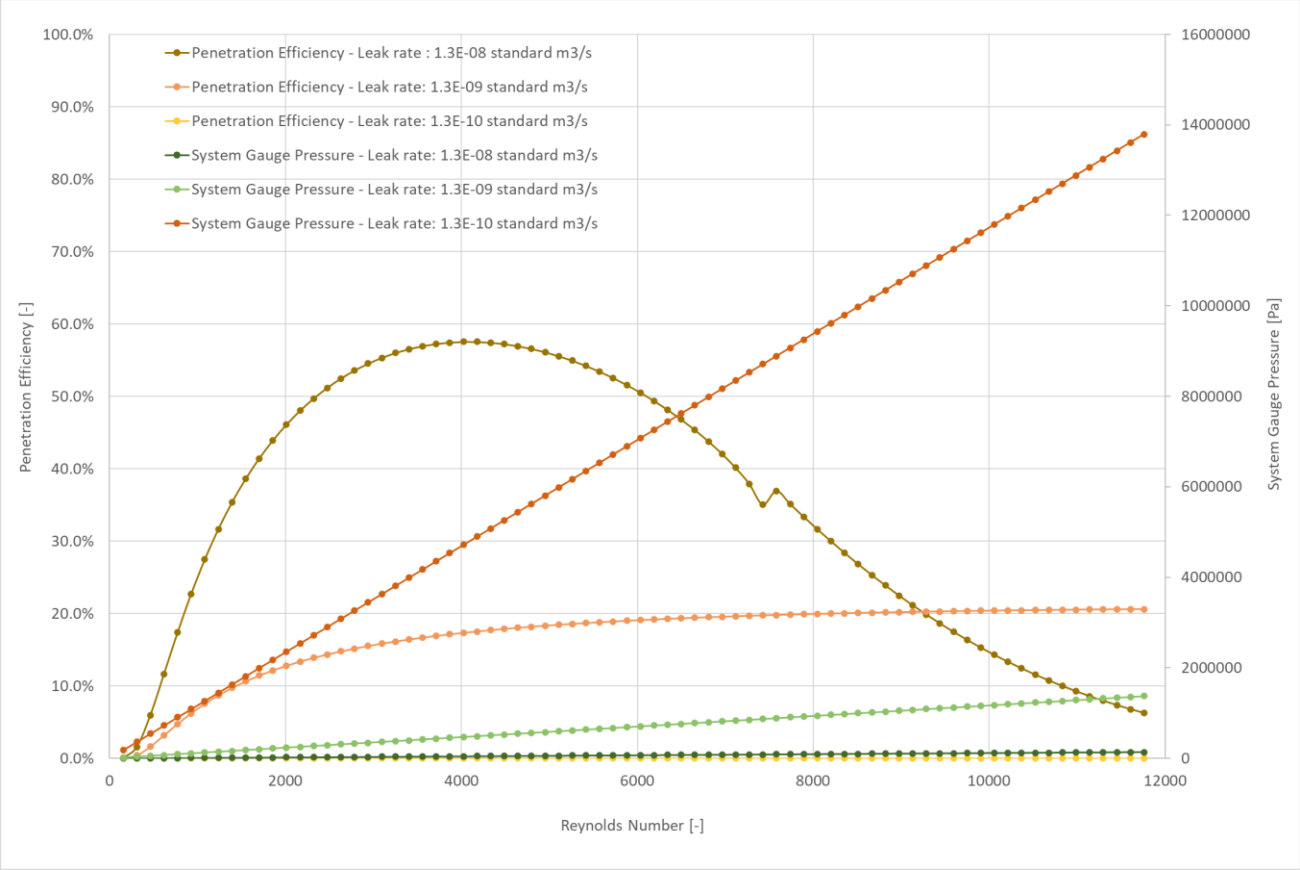

Figure 3.20 The effect of changing leak rates on the Penetration Efficiency and System Gauge Pressure when particles of mass mean diameter 5 µm are injected into a pipe of diameter 12.7 mm (Without pressure relief)

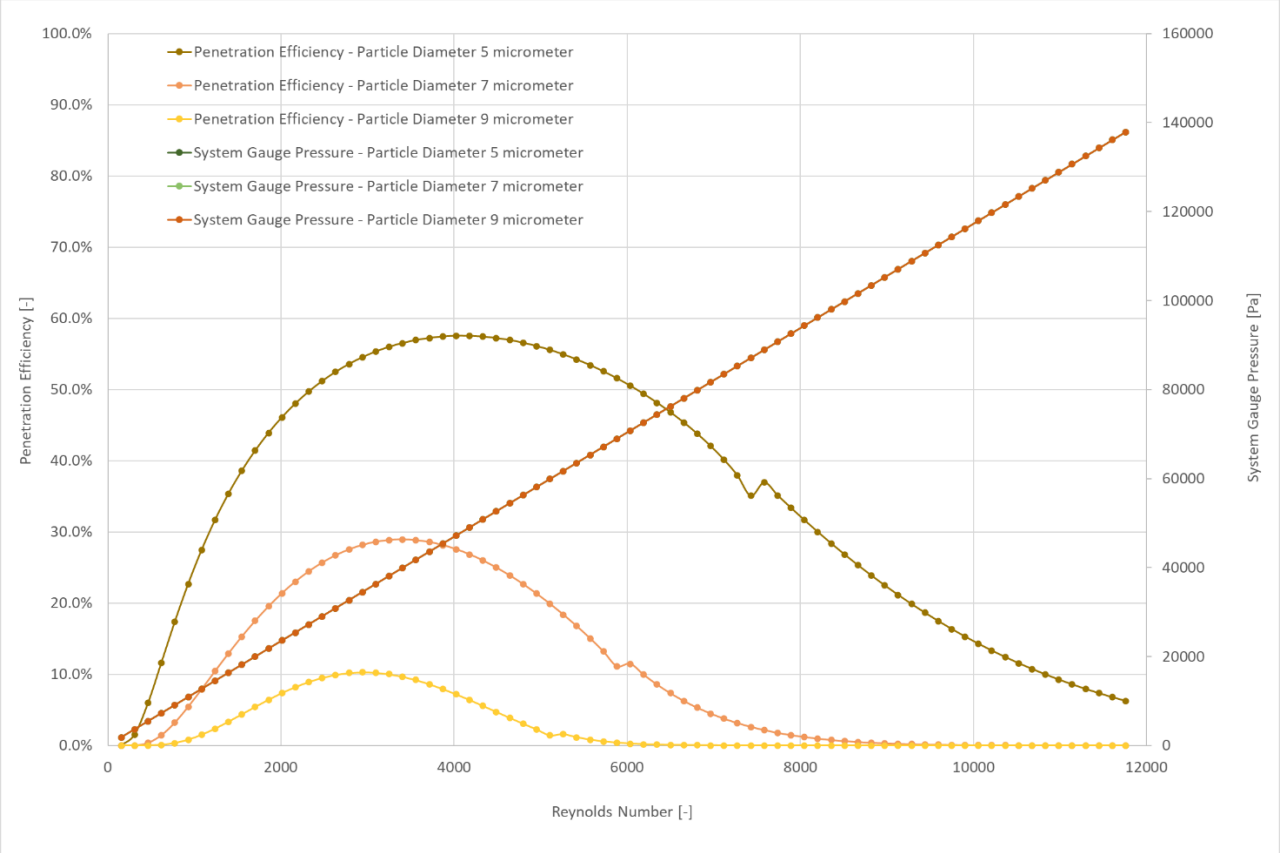

Figure 3.21 The effect of changing particle mass mean diameters on the Penetration Efficiency and System Gauge Pressure when the particles are injected into a pipe of diameter 12.7 mm and leakage rate of 1.3E-08 m^3/s (Without pressure relief)

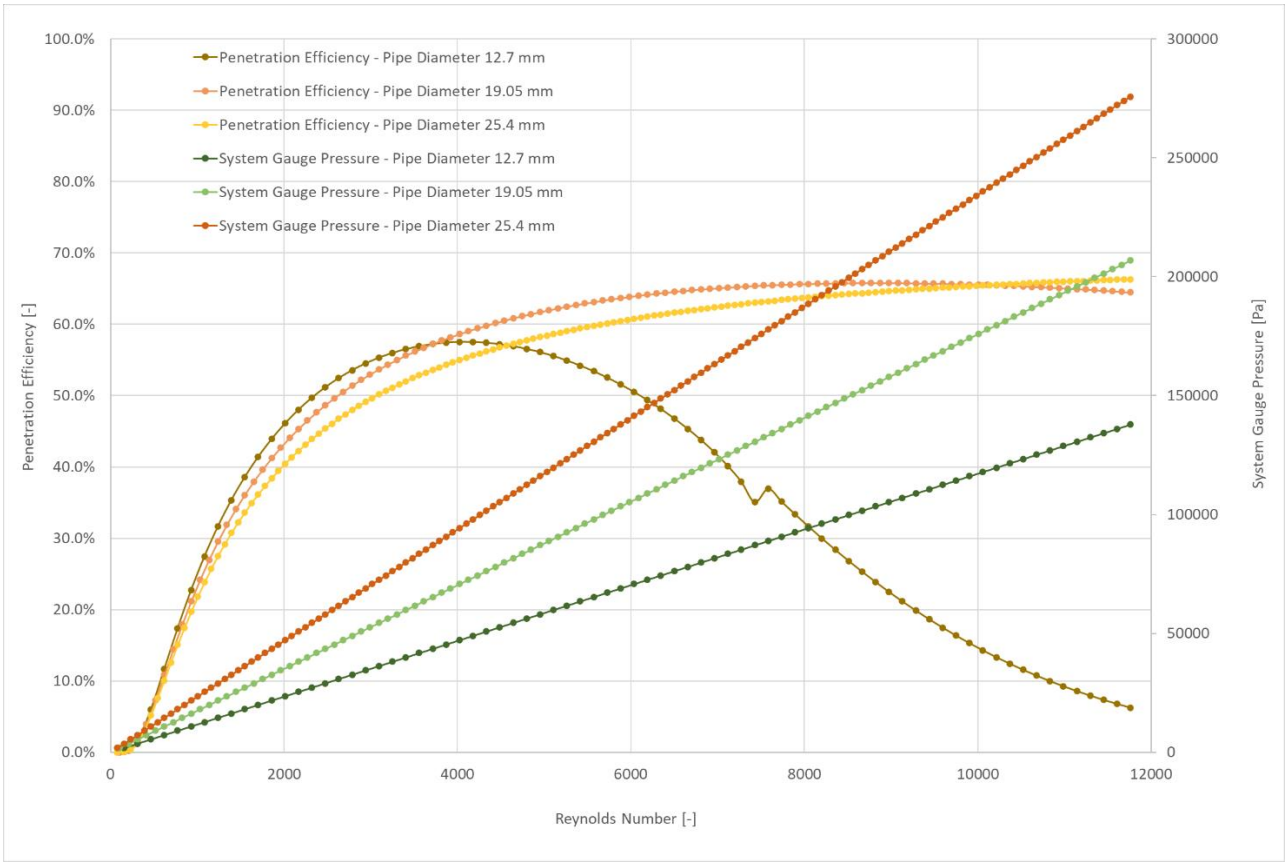

Figure 3.22 The effect of changing pipe diameters on the Penetration Efficiency and System Gauge Pressure when particles of mass mean diameter 5 µm are injected into a pipe of diameter 12.7 mm and leakage rate of 1.3E-08 m^3/s (Without pressure relief)

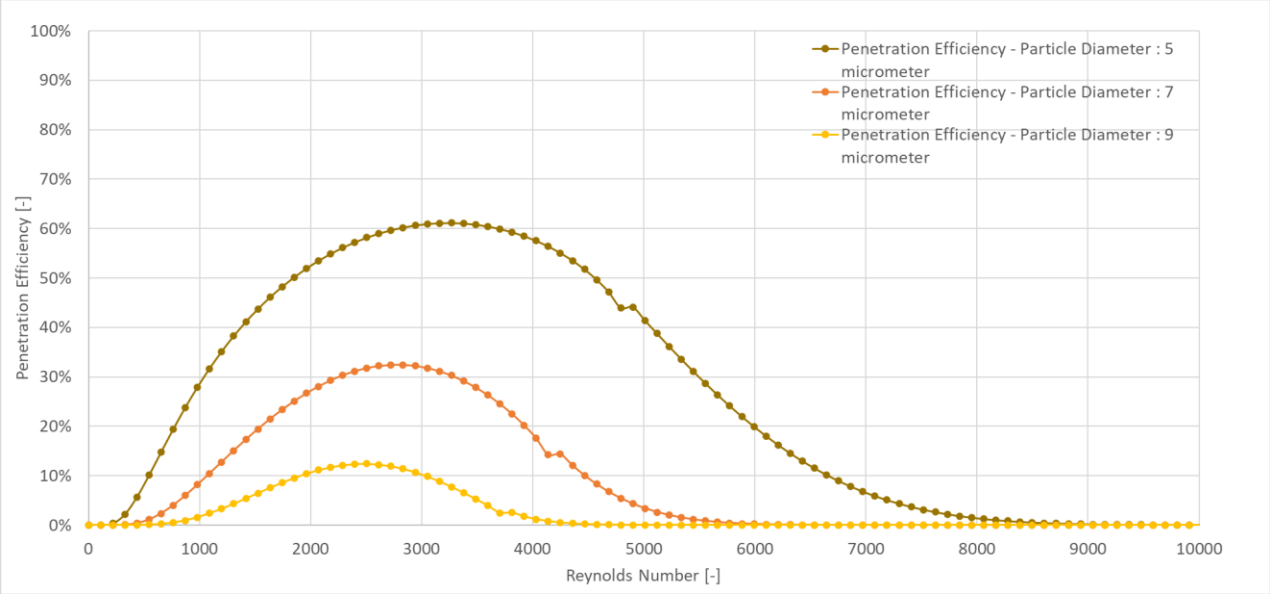

Figure 3.23 The effect of changing particle mass mean diameters on the Penetration Efficiency when the particles are injected into a pipe of diameter 12.7 mm (With pressure relief)

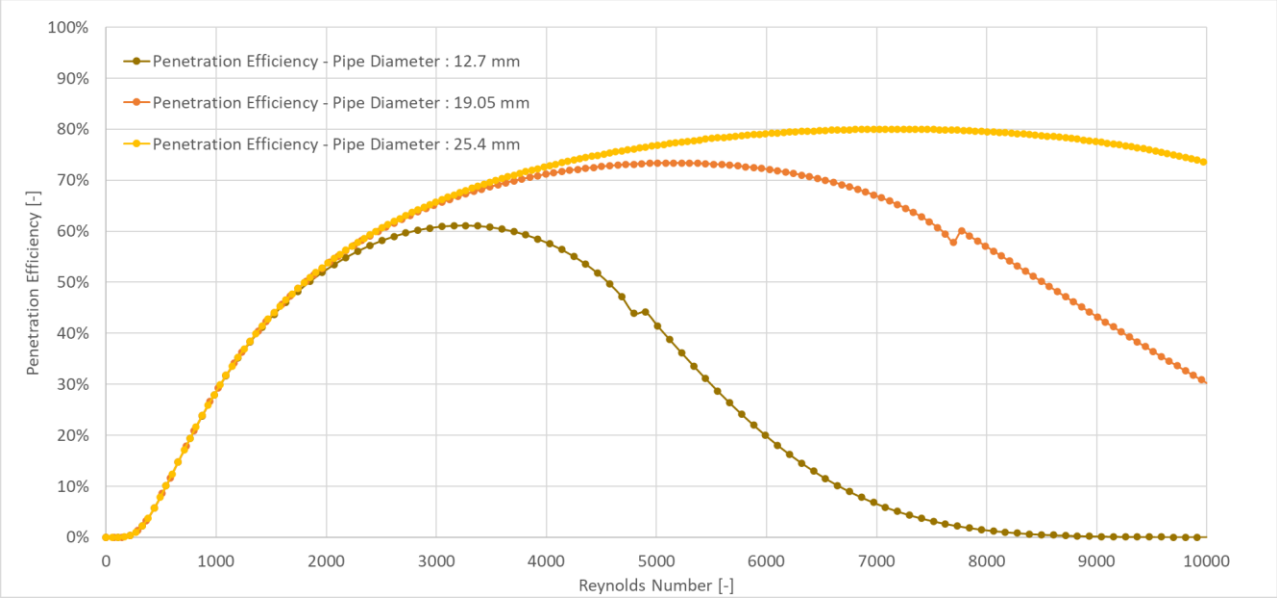

Figure 3.24 The effect of changing pipe diameters on the Penetration Efficiency when particles of (With pressure relief)

3.2.2 Comparison of model results with a previous experimental study

The results of the Anand and McFarland penetration model (Anand & Mcfarland, 1989) with pressure relief were compared with results from a previous unpublished pilot effort that investigated the remote sealing of leaks in natural gas systems[2]. Multiple scenarios analyzed in that experimental study were compared with penetration values calculated by the Anand and McFarland model. Cascade impactor tests quantified particle size distribution produced by the experimental facility used in that study: particle mass mean diameter ranged from 1 to 10 μm with means from 2.9 to 6 μm and standard deviations on the order of 1.5 to 2 μm. The study does not mention the standard deviations for individual experiments where particle distributions with a particle mass mean diameter were produced.

Figure 3.25 and Figure 3.26 compare the penetration values for an experiment conducted in a 40 mm (~1.6 $inches$) diameter pipe with a flow rate of 140 LPM (~5 CFM), with mass mean diameters of 3 μm and 5 μm aerosol particles respectively. In both the cases, the model value shows great agreement with all the experimental values.

The study also noted that the developing section has a large impact on the particle size at the beginning and hence different particle sizes were produced when different flow rates were used. With a flow rate of 280 LPM (~10 CFM), particles with a mass mean diameter of 3 μm are produced. In this case, the model overpredicts the penetration values when compared to the experimental values noted in the individual sections (Figure 3.27). When the test was conducted at 700 LPM (~25 CFM), particles with a mass mean diameter of 4.5 μm produced. While the model value agrees well with the experimental results in the 5.5 – 8.25 m section and the 8.25 –

[2] Work was compiled in a final report submitted to the California Energy Commission Energy Innovations Small Grant Program. Please refer to Appendix B. For further inquiries, contact Jean-Pierre Delplanque: (530) 754-6950 – delplanque@ucdavis.edu or Mark Modera: (530) 754-7671 – mpmodera@ucdavis.edu

11 m section, the model slightly overpredicts the value in comparison to the observed experimental penetration values in the first 2 test sections (Figure 3.28).

In an additional set of experiments, the study focused on varying the flow rate while trying to maintain a constant mass mean diameter of 3.1 μm. When a flow rate of 140 LPM (~5 CFM) is used, the penetration values observed in each test section was approximately equal and the model agrees with the observed values (Figure 3.29). On the other hand, when a flow rate of 280 LPM (~10 CFM) is used, the values observed in the 4 test sections are different with the highest penetration being observed in the final test section. The highest penetration values seem to agree with the model-predicted penetration value (Figure 3.30).

A point to be noted is that the penetration values of the pipe network shown in the previous section (Section 3.2.1) is much less compared to this study where the penetration values are quite close to 100%. There are quite a few reasons for this observation: the penetration is calculated for a pipe length of 20 m in section 3.2.1 whereas this section calculates penetration in 2.75 m long sections of piping; the penetration values were calculated for pipe networks with diameters of 12.7, 19.1, 25.4 mm in section 3.2.1 whereas experiments the study referred to in this section conducted experiments on a 40 mm diameter pipe. From the results computed in section 3.2.1, we know that a higher diameter pipe results in a higher penetration value when all other parameters are kept constant. The combined effect of both these differences results in higher penetration values for the scenarios discussed in section 3.2.2 compared to section 3.2.1.

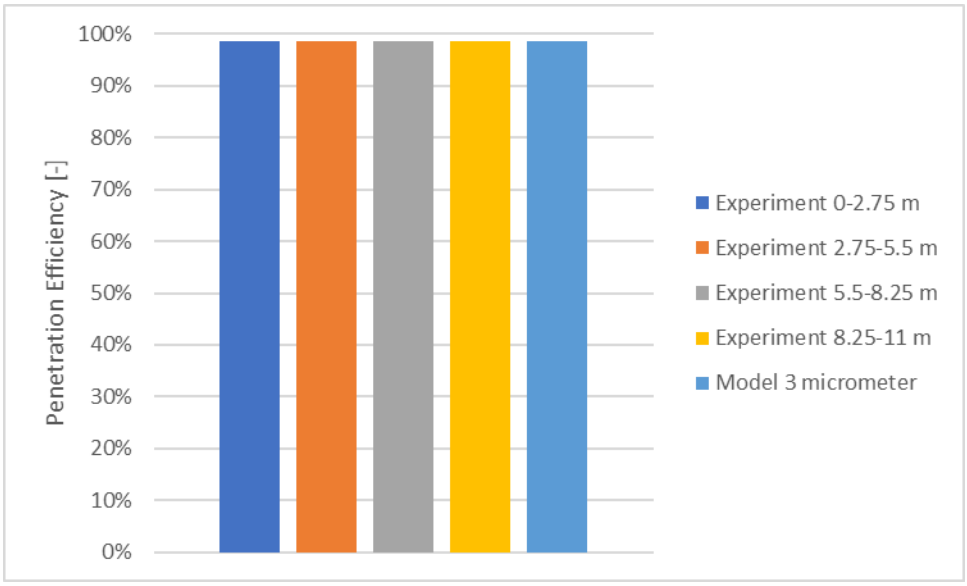

Figure 3.25 Penetration Efficiencies comparing experimental results from consecutive 2.75 m sections of a 40 mm (~1.6- inch) diameter pipe with modelling results from a 2.75 m section of a 40 mm (~1.6-inch) diameter pipe with particles of mass mean diameter 3 µm. The carrier air flow rate is 140 LPM (~5 CFM). The Reynolds number is 4765.

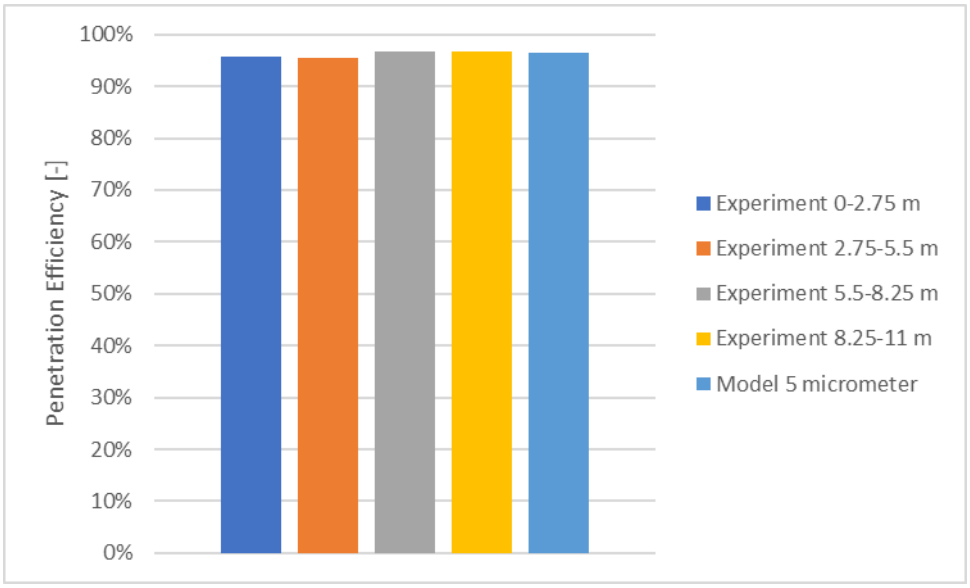

Figure 3.26 Penetration Efficiencies comparing experimental results from consecutive 2.75 m sections of a 40 mm (~1.6- inch) diameter pipe with modelling results from a 2.75 m section of a 40 mm (~1.6-inch) diameter pipe with particles of mass mean diameter 5 µm. The carrier air flow rate is 140 LPM (~5 CFM). The Reynolds number is 4770.

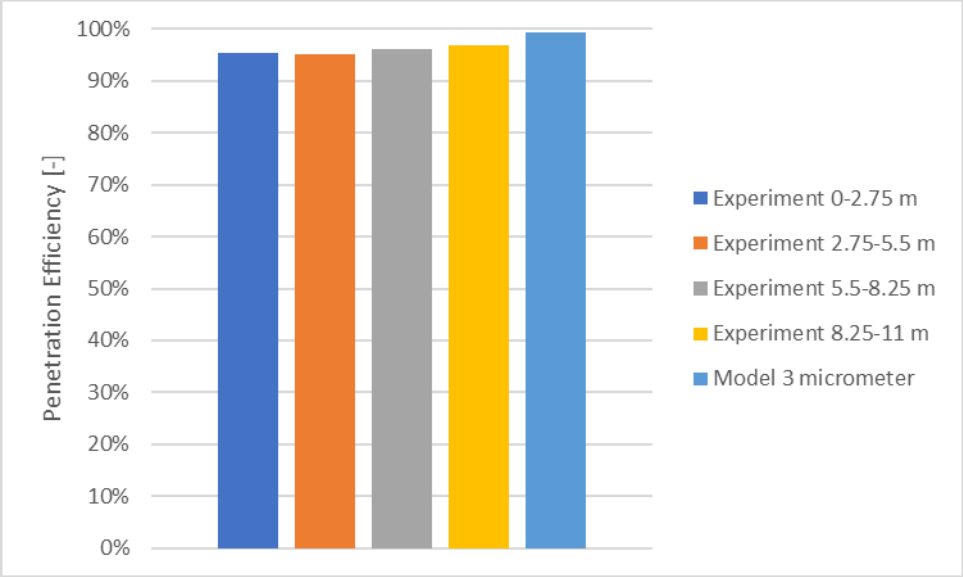

Figure 3.27 Penetration Efficiencies comparing experimental results from consecutive 2.75 m sections of a 40 mm (~1.6- inch) diameter pipe with modelling results from a 2.75 m section of a 40 mm (~1.6-inch) diameter pipe with particles of mass mean diameter 3 µm. The carrier air flow rate is 280 LPM (~10 CFM). The Reynolds number is 9530.

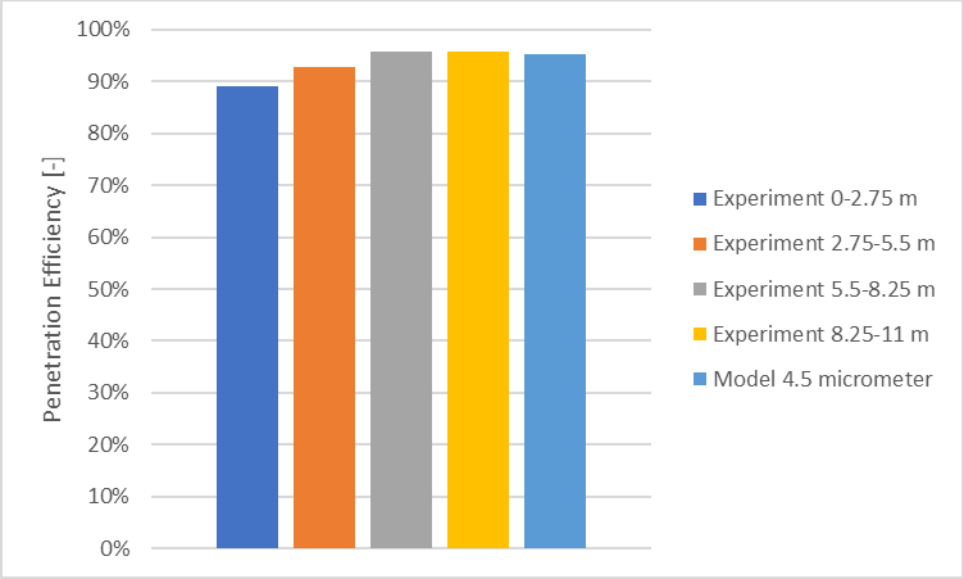

Figure 3.28 Penetration Efficiencies comparing experimental results from consecutive 2.75 m sections of a 40 mm (~1.6- inch) diameter pipe with modelling results from a 2.75 m section of a 40 mm (~1.6-inch) diameter pipe with particles of mass mean diameter 4.5 µm. The carrier air flow rate is 700 LPM (~25 CFM). The Reynolds number is 23830.

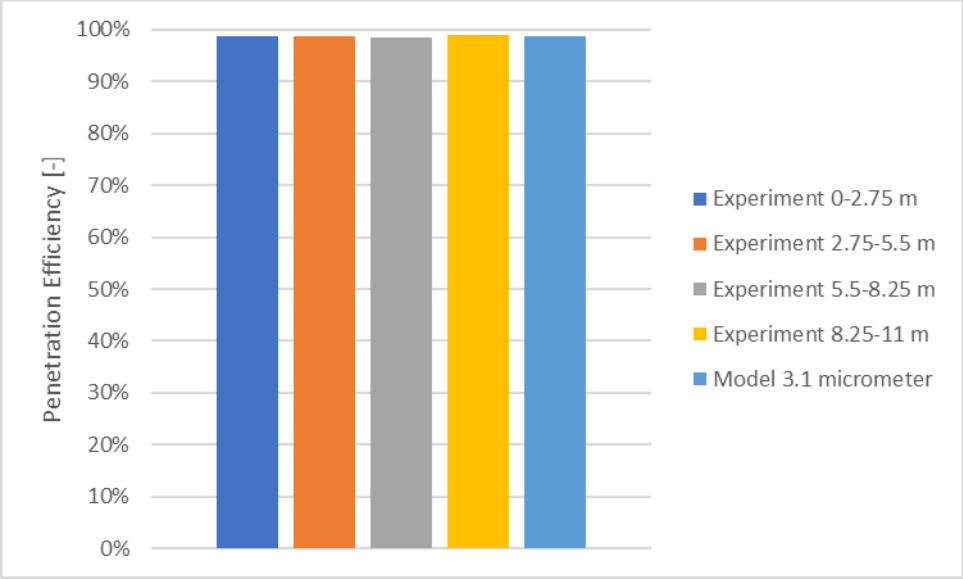

Figure 3.29 Penetration Efficiencies comparing experimental results from consecutive 2.75 m sections of a 40 mm (~1.6- inch) diameter pipe with modelling results from a 2.75 m section of a 40 mm (~1.6-inch) diameter pipe with particles of mass mean diameter 3.1 µm. The carrier air flow rate is 140 LPM (~5 CFM). The Reynolds number is 4770.

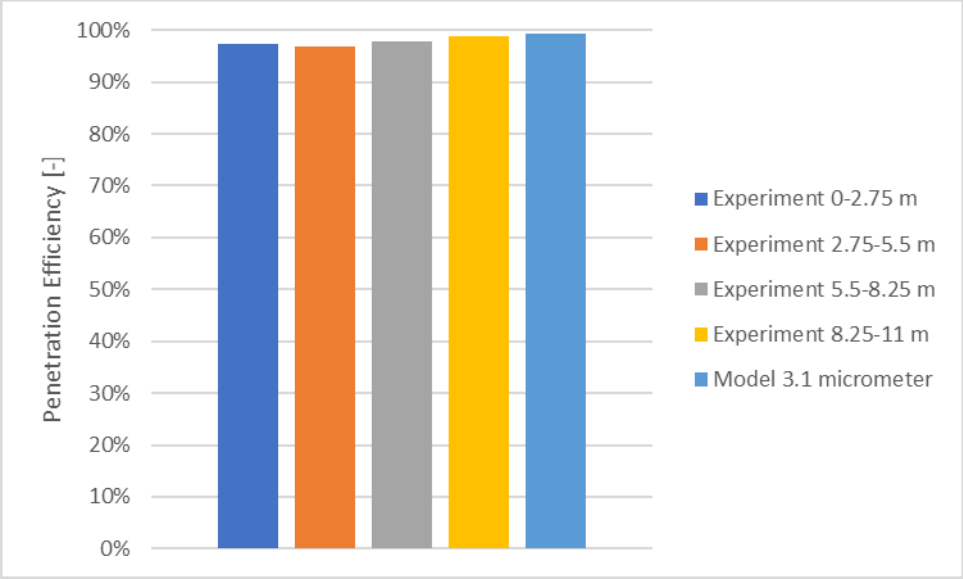

Figure 3.30 Penetration Efficiencies comparing experimental results from consecutive 2.75 m sections of a 40 mm (~1.6- inch) diameter pipe with modelling results from a 2.75 m section of a 40 mm (~1.6-inch) diameter pipe with particles of mass mean diameter 3.1 μm. The carrier air flow rate is 280 LPM (~10 CFM). The Reynolds number is 9530.

3.2.3 Designing the sealing process

Let us consider we have 20 m (~65 ft) of 12.7 mm (0.5 $inches$) piping. Also, let us assume that the average particle size produced by the wand used for spraying the sealant is 8 μm. From Figure 4.1, we can infer that the maximum penetration of 20% that can be achieved for this system is when the Reynolds number of the carrier air flow is set to about 2600. This Reynolds number corresponds to 24 LPM (0.85 CFM) (Figure 3.31).

If we consider another system with 20 m (~65 ft) of 19.1 mm (0.75 $inches$) piping with the same particle size, the max penetration is about 38% at Reynolds number of ~4100. To achieve this value, the required carrier flow is 57 LPM (2 $SCFM$) (Figure 3.32).

In both the above scenarios, the required flow rate is well below the flow rate that can be produced by a compressor at full pressure. For reference, the compressor used in this study produced a flow of 170 LPM (6 CFM) with 6 MPa (90 PSI) compressed air pressure. It is also to be noted that in order to generally produce smaller sealant particles through the wand, it is necessary to increase the compressed air flow rate and lower the sealant flow rate.

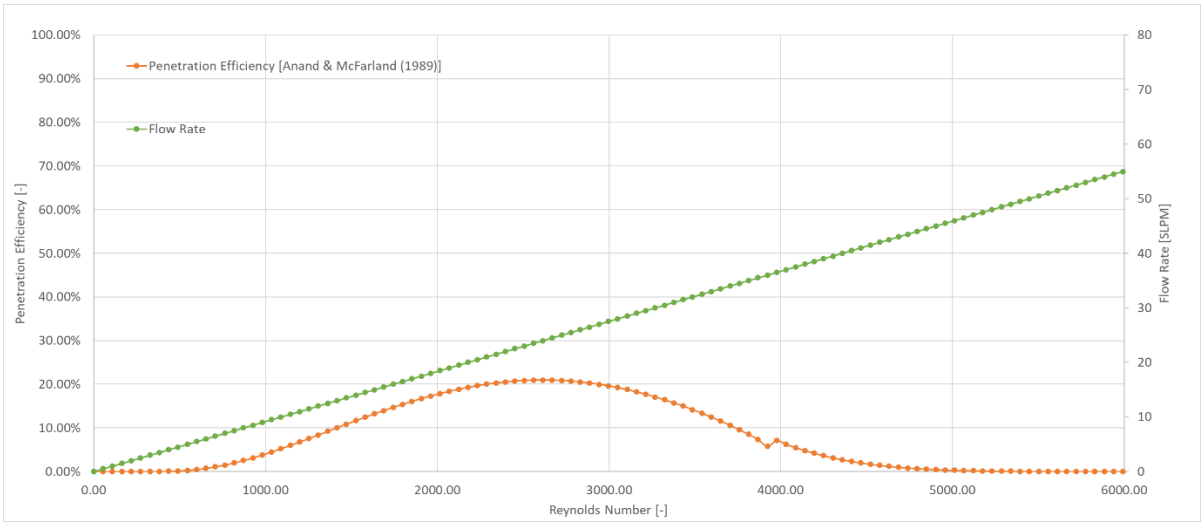

Figure 3.31 Penetration Efficiency and Flow Rate for a system 20 m long with pressure relief [pipe diameter – 12.7 mm; particle diameter – 8 μm]

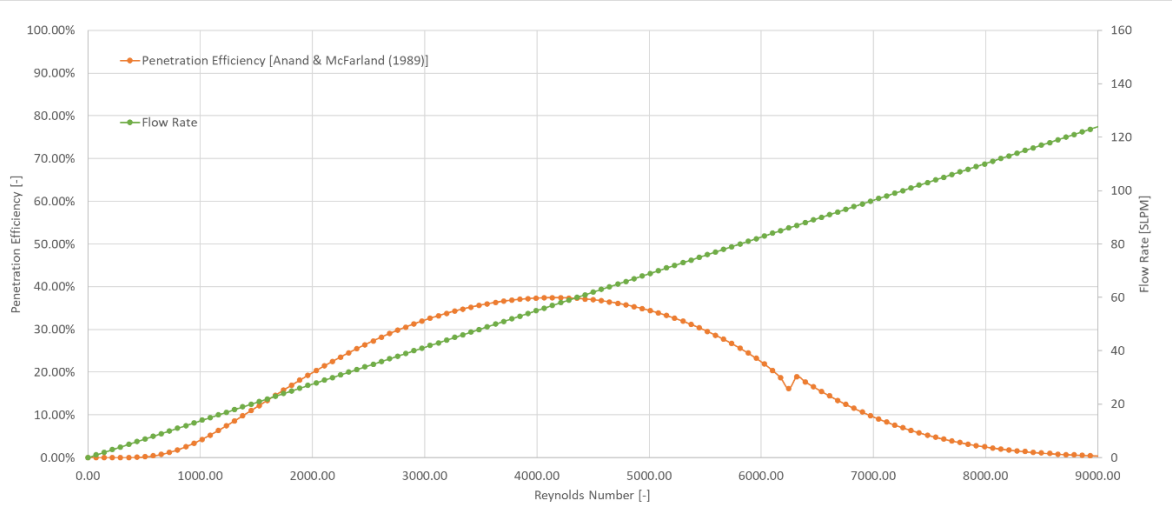

Figure 3.32 Penetration Efficiency and Flow Rate for a system 20 m long with pressure relief [pipe diameter – 19.1 mm; particle diameter – 8 µm]

3.2.4 Actual Sealing results

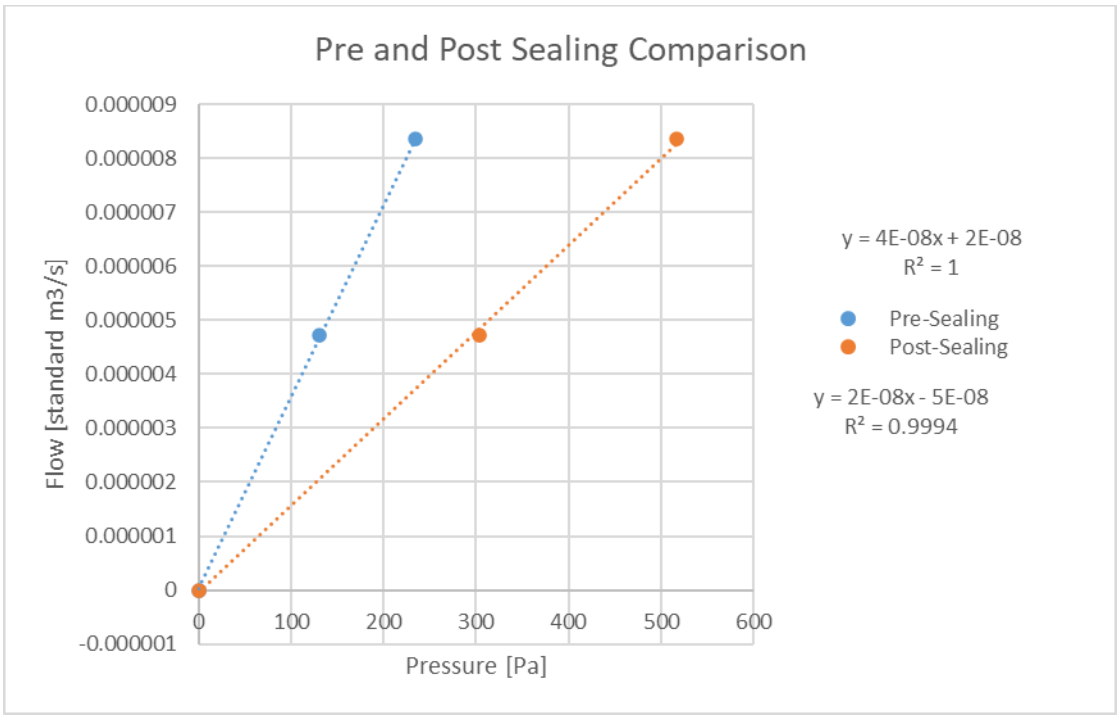

Figure 3.33 Pre- and Post- sealing leakage

The results of the sealing have been reported in Figure 3.33: the leakage rate was reduced by about 55% after the sealing was completed. The leakage rate before sealing was 4E-08 $m^3/s/Pa$ (3460 $mL/day/Pa$) and the leakage rate after the completion of sealing was 2E-08 $m^3/s/Pa$ (1730 $mL/day/Pa$). From the results of the field testing, we know that the highest leakage rate was measured in location 1 and was about 23.2 $standard\ mL/day/Pa$. Thus, the leakage post-sealing is about 74 times the highest leakage measured during the field testing.

a.

b.

c.

d.

e.

f.

g.

i.

j.

Figure 3.34 Pictures of sealed pipes

Figure 3.34 shows the pictures of the components of the pipe network after the sealing was completed. It can be observed that there was significant deposition on the water valve, while the other two valves show little to no observable deposition. The water valve used in the experiment (which was close to the pressure relief cap) was completely blocked because of the sealant, leaving the pressure relief vent useless. It is to be noted that the valve used for the sealing process is not representative of the actual valves used in gas systems.

The pipe sections to which the lay flat was connected did show some deposition. The flexible tubing had no significant deposition although the orifice was small.

The important conclusion from the above sealing test was that although the leakage rate of the test section was halved by the sealing process, the final leakage rate was significantly higher than the leakiest gas networks tested during our field testing.

3.2.5 Measuring the leakage of the sealing apparatus

After completion of the sealing, it was suspected that a possible explanation for the anomalous observations during the sealing experiment was leakage in the apparatus. An experiment was performed to measure the leakage of the apparatus. A leakage of 2.05E-05 $m^3/s/Pa$ (1.77E03 $mL/day/Pa$) was measured. The leakage of the pipe network before the sealing was measured at 4E-08 $m3/s/Pa$ (3.46E03 $mL/day/Pa$), i.e., the leakage of the apparatus was 500 times the leakage of the pipe network. Due to the higher leakage of the apparatus, most of the sealant particles would have preferred to go to the leaks in the apparatus as opposed to the actual pipe network. This could have been a hindrance to the effectiveness of sealing process.

a.

b.

c.

Figure 3.35 Pictures of sealed pipes

4. DISCUSSION

4.1 LEAKAGE DIAGNOSIS

4.1.1 Effect of temperature and barometric pressure changes

Over the course of our testing of 10 systems the procedure evolved. After the third test we decided to run two separate tests, one including flexible connector lines, and one without. Many of the systems did not have enough leakage to be measurable with our protocol: only 2 out of the 10 systems tested had measurable leakage rates. In brief, after isolating the pipe network from the natural gas supply system, the pressure in the network would rise rather than decay. The explanation for this appears to be that the surrounding air temperature was rising, which would cause the pressure in a sealed system to rise. This hypothesis was investigated by spraying water on a wall containing vertical pipe runs or by placing a bag of ice on a pipe section (or both) in 5 of the locations tested. In 4 out of 5 cases the measured pressure dropped, and then resumed its rising pressure trajectory afterwards; in all 4 of these scenarios, cold water was sprayed on the walls with gas piping or on the exposed piping. In the one case where the pressure drop was not observed, only a bag of ice was placed on a small, exposed section of piping; it was suspected that there was not enough thermal mass to produce sufficient heat transfer that would result in a considerable drop in gas temperature and hence gas pressure.

While it is understood that a larger variation in the outside air temperature results in a larger variation in the gas temperature, the fact that gas piping passed through various portions of the house/building, all of which were exposed to different temperatures makes it difficult to exactly predict the influence of outside air temperature on the gas temperature. Since the procedure for diagnosing a potential leak in the system is essentially based on the observation of a pressure

decay, the influence of outside air temperature on the gas temperature becomes an inherent challenge when diagnosing the leakage rate.

An analysis was performed to estimate the equivalent temperature increase of the gas that would nullify or counteract the decrease in pressure due to a leak in the system. The pressure decay for a given system leak rate and volume was calculated using Equation 2.24. Using the ideal gas law, the temperature change that corresponded to a given pressure change was calculated. The results have been tabulated in Table 4.1. As expected, leakier gas systems decay more over a given period and as a result, a larger change in gas temperature is required to nullify the decay. On the contrary, a gas system that is less leaky needs a smaller temperature change to counteract the decay. Even if the temperature change in the gas is only a quarter of the calculated equivalent temperature change, it would be enough to distort the results. The leakage thus calculated would be erroneous and a correction factor must be introduced. But accurately measuring the temperature of the natural gas system is both impractical and strenuous because the temperature would significantly vary depending on the location of the pipe in the house: whether the gas pipe, for example, is in the attic versus if it was the hallway would greatly influence the temperature of the gas in the system.

Location	Pressure Decay in 1 hour (Pa)	Equivalent Temperature Change (K)
1	1386	4
2	848	2.5

Table 4.1 Equivalent Temperature Change Corresponding to Observed Pressure Decay Values

In addition to the temperature change over the course of the day, the change in the barometric pressure due to worsening weather conditions can also affect the measured pressure. For the worst-case scenario of a severe storm front, the barometric pressure changes as much as 206 Pa. This would especially affect systems that are less leaky. Thus, the change in barometric pressure

becomes significant if the gas temperature is constant and the decay due to leakage in the system is less than 200 Pa.

4.2 LEAKAGE SEALING

4.2.1 Modeling wise

The penetration model used for analysis in this study assumes a horizontal tube of a given length. Actual gas networks are more complicated and can include but are not limited to sections of inclined tubing, bends and t-sections. Even with inclined tubing, the effect of gravitational deposition differs depending on whether the laminar pipe flow is inclining or declining; this also includes the case of vertical tubing as well. In the case of bends or t-sections, particle deposition occurs because of inertial impaction; while the lighter particles have a higher tendency to follow the carrier air flow through the bends, the heavier particles have more inertia and escape from the streamlines to impact the walls of the tube and thereby deposit. When designing the sealing procedure for real systems it is important to include the above effects in the model to predict a realistic penetration efficiency value. That analysis is beyond the scope of our effort.

Deposition efficiency was defined in (Carrié & Modera, 1998) as the fraction of particles that deposit on the edges of the leak in comparison to the total number of particles in the air that passes through the leak. The rest of the particles pass through the leak without depositing. However, (Carrié & Modera, 1998)’s two-dimensional model was developed for particle deposition in a slot leak. In contrast, leaks commonly encountered in natural gas distribution networks are expected to be threaded joints. For such leaks, the trajectory of the air, and therefore the particles, is convoluted, resulting in a high probability that most of the sealant particles are deposited somewhere in the joint. This would yield a 100% deposition efficiency according to the above definition. However, deposition is likely to occur such that some sealant is not deposited in the original flow stream through the leak. Another way to look at this is that the cross-sectional area of the ultimate seal can be much larger than the cross-sectional area of

the leak. This can be visualized by comparing the seal on the left side of Figure 4.1 with the seal on the right side of Figure 4.1. Hence, to be able to better capture the deposition at joint leaks, an alternate definition of deposition efficiency is required.

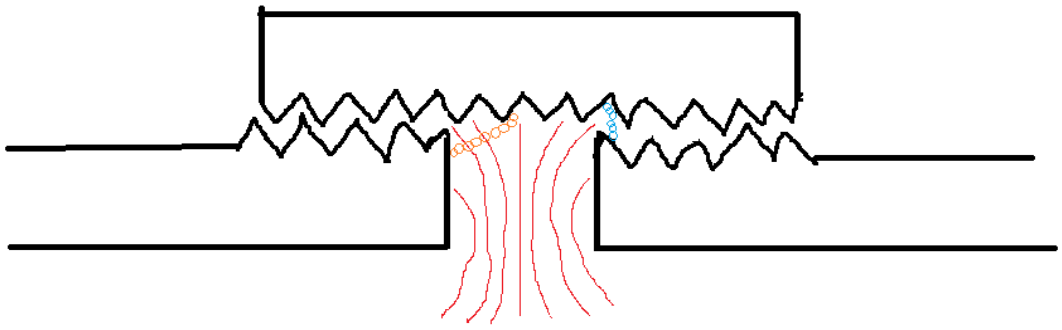

Figure 4.1 Deposition streamlines in joint leaks

Consider a joint leak as shown in *Fig 4.1*. The red curves indicate a fraction of the streamlines that the sealant particles follow along to be deposited. There are two possible modes for the leaks to be completely sealed; these are indicated using orange and blue bubbles. One mode is represented with blue bubbles, in which the sealant particles to enter the threaded region between the pipe and the joint and deposit at the threaded junction. In the second mode, a barrier could be formed by sealant particles that do not enter the threading, but rather deposit on the walls outside of the threaded region between the pipe and the joint, as shown by the orange bubbles. A simplistic model to represent the sealing time in such cases would be as follows:

$$Time\ to\ seal = (Leak\ area * seal\ thickness * seal\ density * (seal/leak\ area\ ratio))/(Sealant\ concentration[kg/m3] * penetration * airflow\ through\ leak * Deposition\ efficiency) \quad (4.1)$$

4.2.2 Equipment wise

In addition to the above discussed shortcomings with the model used in this effort, the use of more sophisticated equipment than what was used in this study can help produce higher penetration efficiencies.

The wand which was used to aerosolize the sealant produces particles with an average diameter of 6 μm. The general trend predicted by the modeling is that smaller particles have a higher penetration efficiency. Thus, if the apparatus was able to produce smaller particles, then better penetration efficiencies can be achieved.

Moreover, in the two scenarios considered while designing the sealing process in section 3.2.3, the flow rate corresponding to maximum penetration was 24 LPM (0.85 CFM) and 57 LPM (2 CFM). But in the apparatus the author used for sealing, the wand acts as both a source of sealant particles and the carrier air. Because a higher compressed air pressure is required to produce smaller sealant particles, the flow rate is inherently maintained on the higher end. Here's an estimate: with a 6 MPa (90 PSI) compressed air pressure, a flow of 170 LPM (6 CFM) can be produced with the compressor we are using. As a thumb rule, the compressor pressure is kept at the maximum limit while reducing the sealant pump flow to minimize the particle size. Thus, the flow rate of air is higher than the prescribed flow for maximum penetration. As a result,

penetration efficiencies are lower and sealing time would increase. It would be ideal if the equipment could produce lower flows while still producing smaller particles.

4.2.3 Proposing a method to seal real gas networks

Consider a single-family residence with 6 appliances connected to the natural gas system (Figure 4.2) with about ~60 m (200 ft) of natural gas running between them and a mix of both 19.1 mm (3/4 $inches$) and 25.4 mm (1 $inches$) piping. As shown in Figure 4.2, the sealant should injected through the piping next to each appliance. Instead of choosing the piping connected to one of the appliances as a pressure relief vent, the piping on the house side should be detached from the meter and left open to atmosphere. This method of releasing sealant to the atmosphere avoids releasing the sealant indoors and creating deposits inside the house. Listed below are the list of components that will be necessary to accomplish the gas system sealing:

- Fan: Controls the flow rate of the incoming air
- Heater: Heats the incoming air and maximize its moisture(sealant) holding capacity
- Wand: Mixes compressed air flow with sealant pump flow, heats the resultant flow, and injects aerosolized particles in the airstream
- Development section: Made of lay flat tubing and allows for the sealant particles to mix with the airstream to achieve a uniform concentration

- Connecting Box: Provides a transition between the large lay flat development section and smaller lay flat tubing that branch to the various appliances

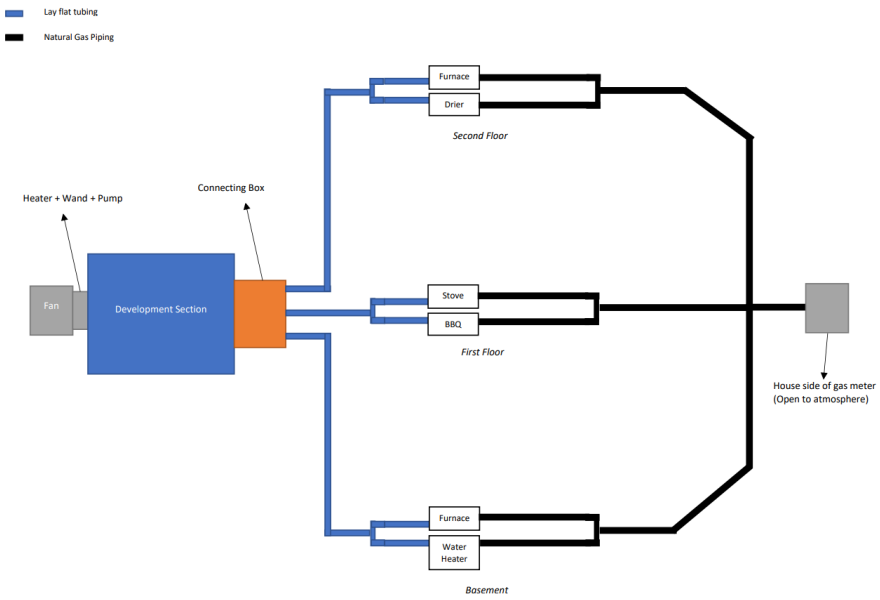

Figure 4.2 Sealing schematic

Procedure:

1. Perform a leak test before sealing to measure baseline leakage
2. Identify appliances connected to the gas line
3. Close burner valves, if any
4. Turn off pilot lights, if any
5. Turn off the main gas supply valve
6. Identify a suitable place for keeping the sealing apparatus
7. Apparatus the controls and electronics for the sealing
8. Connect the lay flat tubing from the connecting box to the piping upstream of the different appliances
9. Turn on the fan box and the compressed air

10. Turn on the heater and the wand
11. Calculate the maximum possible sealant flow rate for the inlet conditions (LabVIEW code)
12. Reduce to a fraction of the maximum sealant flow rate to ensure smaller particles are produced
13. Run for ~20 minutes
14. Cap the pipe on the house side of the meter
15. Remove the lay flat tubing at each appliance and
16. Perform a leak test after sealing to measure new leakage levels and efficiency of the sealing process

5. CONCLUSION

The key take-away from characterizing the leakage of residential natural gas systems is that the expected decay associated with any leakage was so small as to be masked by gas temperature variations in 8 out of 10 cases. Our testing indicates that we can find leakage in flexible lines/connectors, and visual observations using bubble solution indicated that at least one old-style shut-off valve leaks.

The sealing of the make-shift network reduced the leakage by almost 50%, but the absolute leakage post-sealing was still 74-times the highest leakage rate measured during the field testing. Thus, the aerosol process used to seal ducts appears to be capable of sealing leaks in natural gas distribution pipes but will require more refinement to be able to address the low levels of leakage observed in this study. The penetration model employed in the design process only considered horizontal tubes, but to design the sealing process for real systems the penetration through inclined tubing, bends and t-sections needs to be taken into account. Additionally, the deposition at the joint leaks was assumed to be 100% for the sake of analysis, but due to the unique nature of joint leaks, there is further scope for model development to understand the deposition in these leaks. The apparatus used for sealing gas systems could also be further improvised to produce smaller particles and lower air flow rates to enhance particle penetration.

Overall, while the aerosol sealing technology has been successfully commercialized for sealing duct systems, it is still in the early stages of development for natural gas distribution networks. But if the technology comes to fruition, then it may have a huge impact on cutting down CH_4 emissions originating from the residential natural gas systems and thereby helping California achieve its goal of cutting down GHG emissions 40% below 1990 levels by 2030.

REFERENCES

Agarwal, J. K. (1975). *Aerosol Sampling and Transport.* [Ph.D., University of Minnesota]. https://www.proquest.com/docview/302760983/citation/8C5FF58451DD4728PQ/1

Allen, D. T., Torres, V. M., Thomas, J., Sullivan, D. W., Harrison, M., Hendler, A., Herndon, S. C., Kolb, C. E., Fraser, M. P., Hill, A. D., Lamb, B. K., Miskimins, J., Sawyer, R. F., & Seinfeld, J. H. (2013). Measurements of methane emissions at natural gas production sites in the United States. *Proceedings of the National Academy of Sciences*, *110*(44), 17768–17773. https://doi.org/10.1073/pnas.1304880110

Anand, N. K., & Mcfarland, A. R. (1989). Particle Deposition in Aerosol Sampling Lines Caused by Turbulent Diffusion and Gravitational Settling. *American Industrial Hygiene Association Journal*, *50*(6), 307–312. https://doi.org/10.1080/15298668991374714

Anand, N. K., McFarland, A. R., Kihm, K. D., & Wong, F. S. (1992). Optimization of Aerosol Penetration through Transport Lines. *Aerosol Science and Technology*, *16*(2), 105–112. https://doi.org/10.1080/02786829208959541

Carrié, F. R., & Modera, M. P. (1998). Particle Deposition in a Two-Dimensional Slot from a Transverse Stream. *Aerosol Science and Technology*, *28*(3), 235–246. https://doi.org/10.1080/02786829808965524

Carrié, F. R., & Modera, M. P. (2002). Experimental investigation of aerosol deposition on slot- and joint-type leaks. *Journal of Aerosol Science*, *33*(10), 1447–1462. https://doi.org/10.1016/S0021-8502(02)00086-1

Fischer, M. L., Chan, W. R., Delp, W., Jeong, S., Rapp, V., & Zhu, Z. (2018). An Estimate of Natural Gas Methane Emissions from California Homes. *Environmental Science & Technology*, *52*(17), 10205–10213. https://doi.org/10.1021/acs.est.8b03217

Harrington, C., & Modera, M. (2013). *Achieving and Certifying Building Envelope Air Tightness with an Aerosol-Based Automated Sealing Process*. 8.

Harrington, C., & Modera, M. (2014). Recent Applications of Aerosol Sealing in Buildings. *International Journal of Ventilation*, *12*(4), 345–358. https://doi.org/10.1080/14733315.2014.11684028

Hendrick, M. F., Ackley, R., Sanaie-Movahed, B., Tang, X., & Phillips, N. G. (2016). Fugitive methane emissions from leak-prone natural gas distribution infrastructure in urban environments. *Environmental Pollution*, *213*, 710–716. https://doi.org/10.1016/j.envpol.2016.01.094

Lamb, B. K., Cambaliza, M. O. L., Davis, K. J., Edburg, S. L., Ferrara, T. W., Floerchinger, C., Heimburger, A. M. F., Herndon, S., Lauvaux, T., Lavoie, T., Lyon, D. R., Miles, N., Prasad, K. R., Richardson, S., Roscioli, J. R., Salmon, O. E., Shepson, P. B., Stirm, B. H., & Whetstone, J. (2016). Direct and Indirect Measurements and Modeling of Methane Emissions in Indianapolis, Indiana. *Environmental Science & Technology*, *50*(16), 8910–8917. https://doi.org/10.1021/acs.est.6b01198

Modera, M. P., & Carrie, F. R. (1999). *Method for Sealing Remote Leaks in an Enclosure using an Aerosol* (Patent No. 5,980,984).

Modera, M. P., Dickerhoff, D., Nilssen, O., Duquette, H., & Geyselaers, J. (1996). *Residential Field Testing of an Aerosol-Based Technology for Sealing Ductwork*. 7.

APPENDIX A.

The following is an excerpt from 'Abstract' section of the final report submitted to the 'Energy Innovations Small Grant Natural Gas Program':

Although there are technologies that address leaks in natural-gas transmission lines from the inside, the state of the art for small-diameter low-pressure sections of natural gas distribution systems involves exterior identification of leakage site(s) followed by excavation and installation of an exterior seal. The objective of this project was to investigate a less invasive procedure that locates and seals leaks from inside small-diameter pipes using an aerosolized sealant. This effort proved experimentally that an interior aerosol process can seal 1/8–inch diameter leaks in 1.6-inch diameter pipes within one hour, at least 110 feet from the injection point. Furthermore, the testing demonstrated that the seals produced had minimal residual tack, and could withstand at least 1.4 psi pressure differentials without failing. Experiments also demonstrated the impact of flow rate and particle size on the transport of the aerosolized sealant within pipes, demonstrating sealant-particle loss rates of 1 to 2% per 9 feet of pipe length. A 1.5% loss per 9 feet implies that sealant concentration remains above 50% of the initial value at 400 feet from the injection point. It was demonstrated that higher flow rates and larger particle sizes both resulted in increased wall deposition, as well as that the current sealant material did not dry quickly enough to avoid sealing gas-appliance orifices 175 feet downstream of injection, at least at tested gas flow rates. This suggests that gas appliances would need to be isolated (i.e. inlet valves turned off) during sealing. Finally, computational fluid dynamics simulations were performed for the transport of sealant particles from the injection point to leakage sites. Simulation results were compared with experimental results for 1.6 and 14 inch diameter pipes, showing better agreement at 14-inch and generally over-predicting wall deposition.

APPENDIX B.

The following is an excerpt from ‘Project Outcomes’ section of the final report submitted to the ‘Energy Innovations Small Grant Natural Gas Program’:

- **The numerical model predictions of sealant penetration are within 7% of the experimental observations except for small pipes.**

A numerical model was developed to solve for the fate of particles flowing in a 14-in diameter pipeline. Experimental data (shown in Figure 3) collected with sealant A, which remained tacky even after drying, was used to validate the model predictions of sealant penetration. This choice enables validations of the primary aspects of the model, transport and dispersion, without requiring that evaporation be included. As seen in Figure 3, the second simulation approach, which accounts for the anisotropy of the turbulent velocity fluctuations near the wall as mentioned in the Project Approach section, provided better agreement with the experimental data showing an average error of only 4%. Table 2 summarizes the relative error of the simulation predictions for both models.

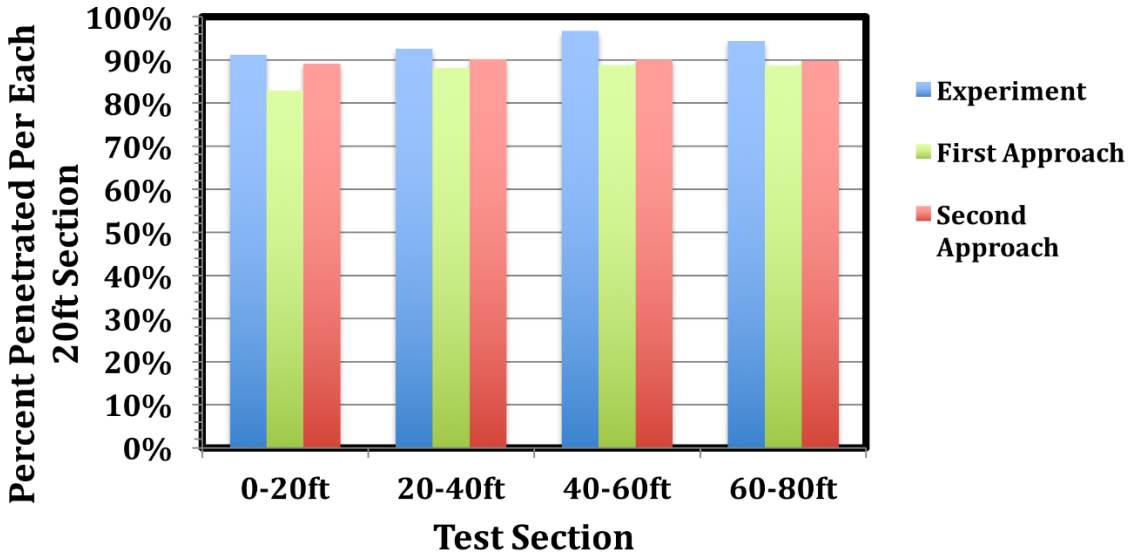

Figure 3: Comparison of two simulations vs. experimental data of the percent aerosol penetration through each consecutive 20-ft sections in the 14-in diameter experiments.

Table 2: Relative error of both first and second approaches relative to experimental data.

	20ft	40ft	60ft	80ft	**Average**
First Approach	9.12%	4.85%	8.20%	6.15%	**7.08%**
Second Approach	2.27%	2.63%	6.86%	4.93%	**4.17%**

Preliminary measurements in a 14-in diameter pipe were acquired for the purpose of comparison with the numerical simulation results. This experimental data is shown in Figure 3. The experiment was conducted using airflow rates of 50-cfm (Reynolds number of 5000), sealant injection at 5ccm, and air compressor pressure of 80psi leading to MMD of particle size of 5.8 micrometer at the entry of the first 20ft test sections and 4.6 micrometer at the end of the 100ft.

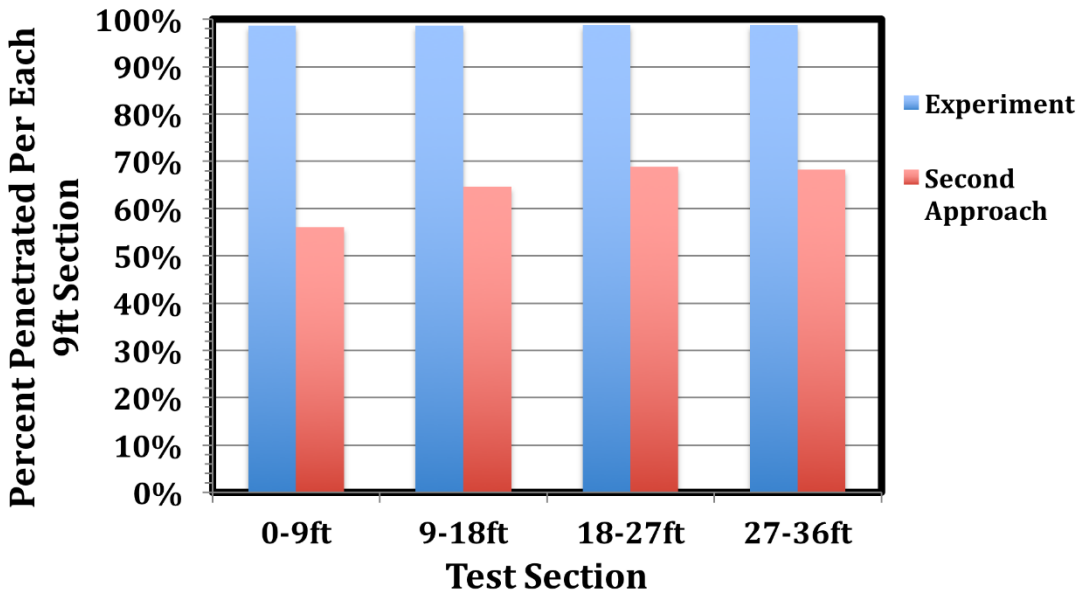

Figure 4: Comparison of simulation (using the Second Approach) and. experimental data of the percent aerosol penetration through each consecutive 20-ft sections in the 1.6-in diameter pipe (flow: 5cfm; particle loading: 1ccm; pressure: 100psi; MMD=3micron).

It is noted that the accuracy of numerical prediction degrades noticeably for small pipe diameters. Figure 4, illustrates that discrepancy with the numerical model underpredicting penetration by over 30%. This discrepancy is attributed to challenges inherent to the resolution of the near-wall region. The challenges encountered with small diameter pipes are representative of the open fluid physics questions in that area.

Because aerosol penetration and wall deposition are closely connected, the two following outcomes are combined in the discussion below;

- **The aerosol penetration length (defined as the distance from injection at which at least 75% of the aerosol has not deposited) could be varied by as much a 7 fold by varying process conditions (e.g. flow, particle size, particle loading, particle drying time).**

- **It was shown that the particle deposition on interior surfaces can be kept s as low as 1-2% per section for certain process conditions. Other configurations exhibited particle deposition as high as 10% per section.**

For both the 1.6-in and 14-in diameter pipes, the concentration loss from the particulate flow to wall deposition was recorded and the results were evaluated based on two methods: cumulative penetration length and sealant deposition on the wall of each lay-flat test sections. The test sections for 1.6-in and 14-in diameter pipes were 9ft and 20ft respectively with each having a total of four sections. Four process parameters were considered: particle size, particle drying, and air flow rate and the effect of each is discussed below.

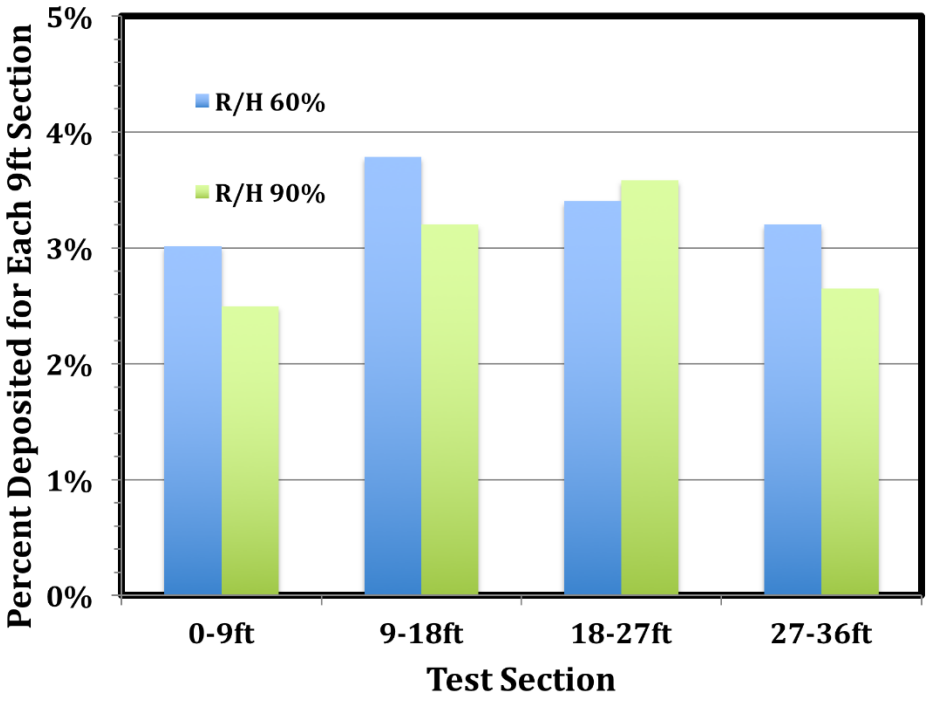

Figure 5: Measured wall deposition for each consecutive 9-ft test section of 1.6-in diameter pipe at two different relative humidity values (60% and 90%) at an airflow rate of 5 cfm, sealant injection rate of 0.36-ccm, and nozzle pressure of 100-psi.

Particle Drying

Sealants B was observed to lose tackiness once completely dried (sealant A does not and was therefore not considered here). Hence, the impact of particle drying on aerosol penetration and wall deposition under varying humidity conditions in the pipeline was measured. The indication of particle drying is based on lower wall deposition and more particle penetration. Figure 5 shows experimental data for wall deposition in each 9-ft section of 1.6-in diameter pipe under two different relative humidity conditions (60% and 90%). Surprisingly, Figure 5 indicates dryer conditions had more sealant deposition on walls than wetter conditions. Tests run at 60% relative humidity had an average of 3.1% deposition per section while tests run at 90% relative humidity

had 2.4% deposition per section. Both tests show less than 10% disposition on interior surfaces. It should be noted that repeatability testing could show this difference to be within the measurement uncertainty, but this testing appears to show that particle tackiness is also sensitive to high relative humidity conditions.

Particle Size

In order to evaluate the impact of particle size, the wall deposition and particle penetration were compared between experiments in which particle size distributions were varied. Each experiment used sealant C (to allow for better visualization), 5 cfm airflow rate, 1 ccm sealant injection rate and 90% relative humidity. Three air compressor pressures were evaluated at 10 psi, 70 psi and 100 psi while holding the sealant injection rate constant in order to create different size particles. The particle size distribution of each case was measured using a cascade impactor. The results show that tests operated with a nozzle pressure of 100 psi and 70 psi both produce similar particle size distributions with an MMD of 3 while tests operated at 10 psi showed particle distributions with an MMD close to 5 (Figure 6).

The wall deposition results for tests with varying particle size exhibited a significant influence of particle size distribution (Figure 7). Tests at 100 psi and 70 psi nozzle pressure, which had similar MMD particle distributions, showed very similar deposition rates while tests performed at 10 psi with larger particles showed a more than three-fold increase in deposition rate. This follows the expected trend since larger particles tend to deposit at higher rates than smaller particles.

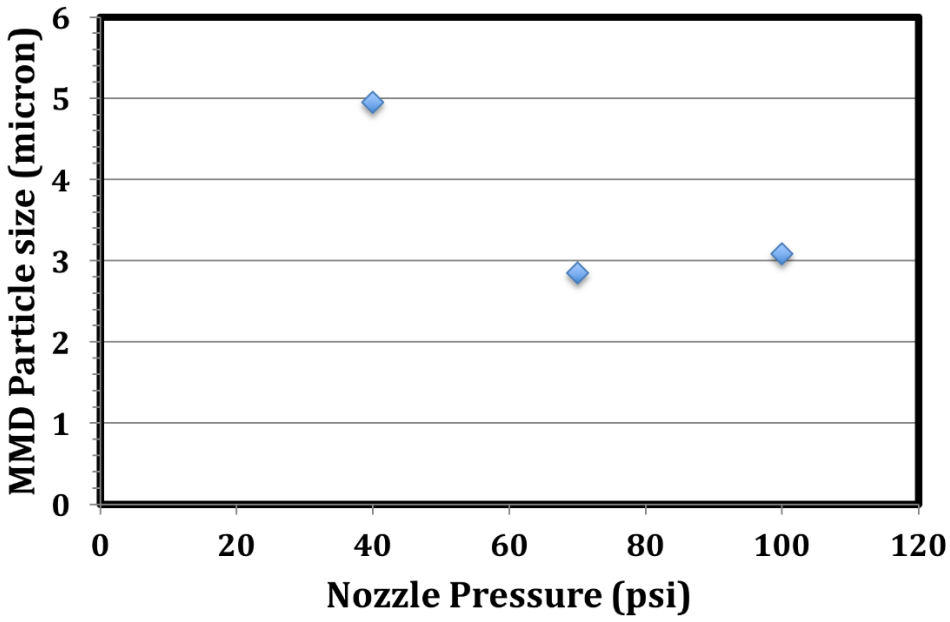

Figure 6: Measured mass mean diameter (MMD) of particles entering the first 1.6-in diameter test section as a function of nozzle air pressure.

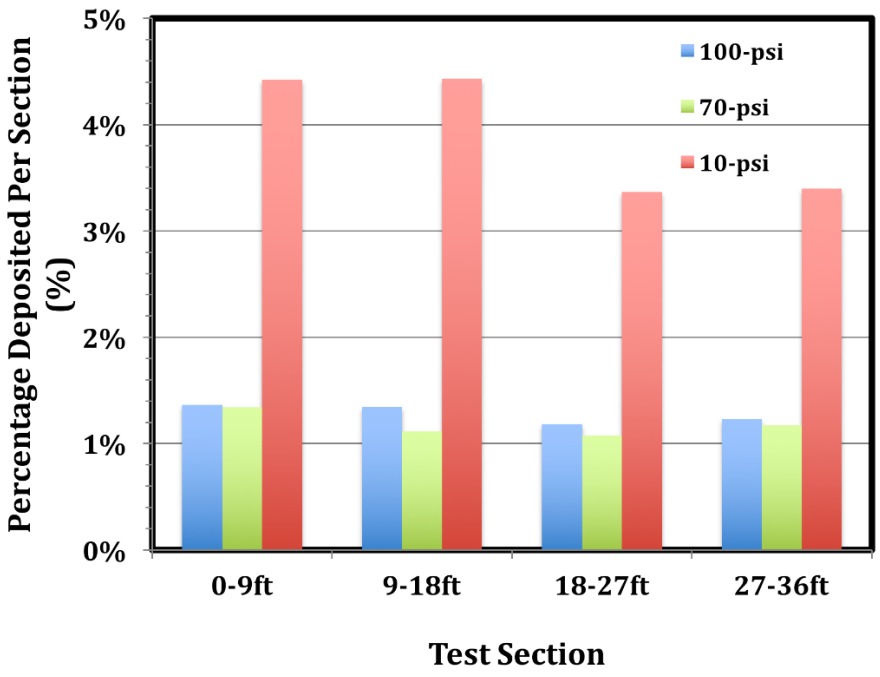

Figure 7: Measured wall deposition for each consecutive 9-ft test section of 1.6-in diameter pipe at three different nozzle pressures (100 psi, 70 psi, and 10 psi) at an airflow rate of 5 cfm, sealant injection rate of 1-ccm, and relative humidity of 90%.

Flow Rate

Initial, experiments were conducted using sealant B to test the sensitivity of air flow rate on particle penetration length and sealant deposition on interior surfaces. Tests were conducted at 10 and 25 cfm with otherwise identical control parameters including air compressor pressure at 100-psi, sealant injection rate 0.36-ccm and relative humidity at 70%; however, testing showed that while the nozzle conditions were held constant the particle size measured in the first test section differed significantly between tests. It became apparent that the developing section had a large impact on particle size distribution at the start of the tests sections resulting in varying particle size distributions between tests at 10 cfm and tests at 25 cfm. Cascade impactor measurements

showed a MMD of 3 microns for tests at 10 cfm and MMD 4.5 microns for tests at 25 cfm. Furthermore, since the tests used the same sealant injection rate, the concentration of sealant in the two tests differed by a factor of 2.5. Figure 8 presents the results showing 25 cfm tests depositing at a higher rate than 10 cfm tests. Unfortunately, based on these tests it was unclear what impact air flow rate alone had on the overall result.

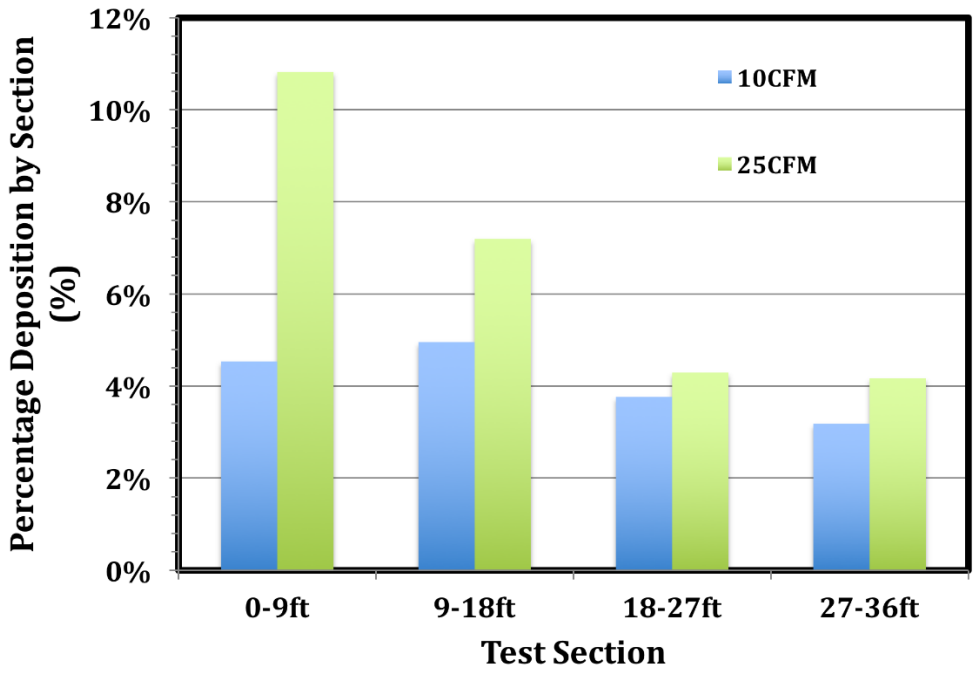

Figure 8: Wall deposition on each test section for 10cfm and 25cfm tests with same nozzle injection parameters of 0.36ccm sealant injection and 100psi compressed air pressure.

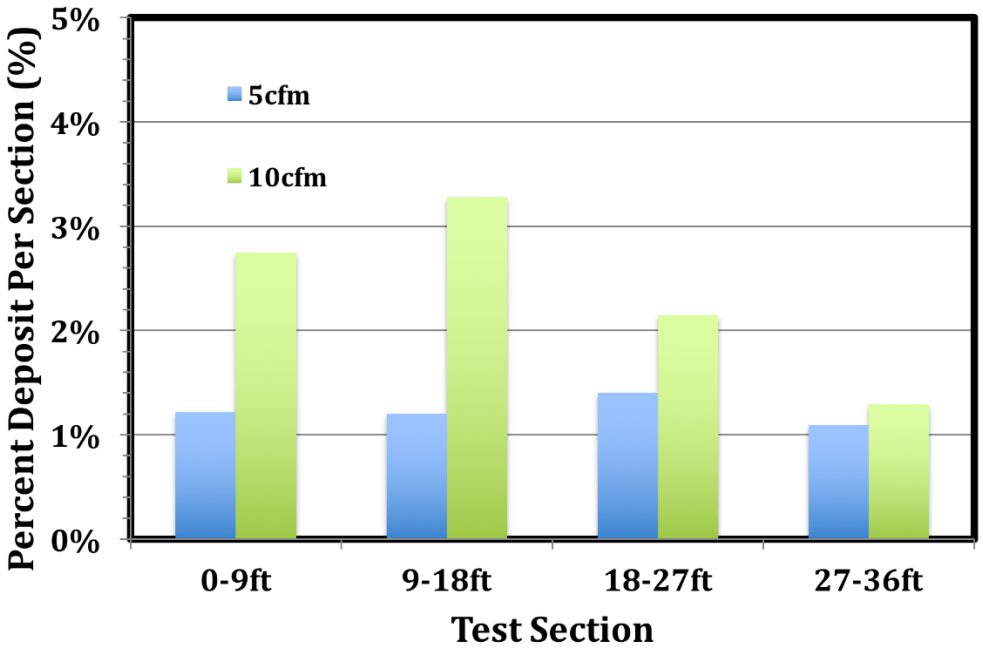

Figure 9: This plot represents the wall deposition per each 9ft sections up to 36ft. This compares the 5 and 10cfm airflow rates at similar particle diameter size 3.1 microns at the first test section

An estimate of the penetration length as defined in the Project Approach section (the distance after injection at which at least 75% of the particles have not deposited yet) can be obtained for the cases shown in Figure 8 and Figure 9. Consider the 25 CFM case shown in Figure 8. The data shows that the sectional fraction of undeposited particles, F_{us}, is 89% after section 1, 93% after section 2, 96% after section 3 and 96% after section 4. Hence at the exit of section 4, 76% (=0.89×0.93×0.96×0.96) of the particle flow rate that entered section 1 has yet to deposit (F_u=0.76) yielding a penetration length on the order of 36 ft. Meanwhile, the data presented in Figure 9 for 5 CFM, shows that the deposition fraction is a significantly more consistent across

sections, at about 1%. Approximating it as constant, the fraction exiting section *n* can be calculated as $F_u = (F_{us})^n$, the section in which less than 75% of the particle entering section 1 is left is given by*: n=log(0.75)/log(0.99) ~ 28, or 252 ft*, which is 7 times larger than the length obtained in the previous case considered.

Additional investigations were performed in an attempt to provide a more comprehensive study of the influence of air flow rate on particle penetration and wall deposition. These experiments focused on maintaining similar particle size distributions in the pipeline. These tests looked at air flow rates of 5 and 10 cfm and particle size distributions with an MMD of 3.1. As seen in Figure 9, there was more than double the particle deposition for tests with the higher air flow rate in the first two sections which then began to converge to a difference of only 0.2% in the fourth test section. One variable that these tests were not able to control was aerosol concentration. The test at 10 cfm air flow rate had twice the aerosol concentration than the test at 5 cfm. The impact of aerosol concentration needs further investigation to separate the impact of air flow and concentration. As reported above, the surface of the plastic lay-flat duct used in these experiments differs from that of gas pipelines. While the influence of that difference on the trends reported here is unlikely to be a first order effect, it should be quantified as part of the steps towards commercialization.